

## Seasonal Climate Predictability in a Coupled OAGCM Using a Different Approach for Ensemble Forecasts

JING-JIA LUO, SEBASTIEN MASSON, AND SWADHIN BEHERA

*Frontier Research Center for Global Change, JAMSTEC, Yokohama, Japan*

SATORU SHINGU

*NEC System Technologies, Ltd., Tokyo, Japan*

TOSHIO YAMAGATA\*

*Department of Earth and Planetary Science, University of Tokyo, Tokyo, Japan*

(Manuscript received 11 November 2004, in final form 9 March 2005)

### ABSTRACT

Predictabilities of tropical climate signals are investigated using a relatively high resolution Scale Interaction Experiment–Frontier Research Center for Global Change (FRCGC) coupled GCM (SINTEX-F). Five ensemble forecast members are generated by perturbing the model's coupling physics, which accounts for the uncertainties of both initial conditions and model physics. Because of the model's good performance in simulating the climatology and ENSO in the tropical Pacific, a simple coupled SST-nudging scheme generates realistic thermocline and surface wind variations in the equatorial Pacific. Several westerly and easterly wind bursts in the western Pacific are also captured.

Hindcast results for the period 1982–2001 show a high predictability of ENSO. All past El Niño and La Niña events, including the strongest 1997/98 warm episode, are successfully predicted with the anomaly correlation coefficient (ACC) skill scores above 0.7 at the 12-month lead time. The predicted signals of some particular events, however, become weak with a delay in the phase at mid and long lead times. This is found to be related to the intraseasonal wind bursts that are unpredicted beyond a few months of lead time. The model forecasts also show a “spring prediction barrier” similar to that in observations. Spatial SST anomalies, teleconnection, and global drought/flood during three different phases of ENSO are successfully predicted at 9–12-month lead times.

In the tropical North Atlantic and southwestern Indian Ocean, where ENSO has predominant influences, the model shows skillful predictions at the 7–12-month lead times. The distinct signal of the Indian Ocean dipole (IOD) event in 1994 is predicted at the 6-month lead time. SST anomalies near the western coast of Australia are also predicted beyond the 12-month lead time because of pronounced decadal signals there.

### 1. Introduction

In the last two decades both understanding and simulation of El Niño–Southern Oscillation (ENSO) have been largely improved (e.g., Neelin et al. 1998; Achutarao and Sperber 2002). Following the first successful

forecast of the 1986/87 El Niño event with a simple coupled model (Cane et al. 1986), significant progress in the ENSO prediction has been achieved using ocean–atmosphere coupled general circulation models (OAGCMs) with various complexities (e.g., Barnston et al. 1999). Existing hierarchy of coupled models include the simple, intermediate, hybrid anomaly coupling; flux-corrected CGCMs; and nonflux-adjusted CGCMs (e.g., Chen et al. 1997; Balmaseda et al. 1994; Barnett et al. 1993; Kirtman et al. 1997; Ji et al. 1994; Stockdale et al. 1998). Experimental ENSO forecasts have been provided on real-time basis for the last decade (see the *Experimental Long Lead Forecast Bulletin* online at <http://grads.iges.org/ellfb/home.html>). Re-

---

\* Additional affiliation: Frontier Research Center for Global Change, JAMSTEC, Yokohama, Japan.

---

*Corresponding author address:* Jing-Jia Luo, Frontier Research Center for Global Change, JAMSTEC, 3173-25 Showa-machi, Kanazawa-ku, Yokohama, Kanagawa 236-0001, Japan.  
E-mail: [luo@jamstec.go.jp](mailto:luo@jamstec.go.jp)

cent results have also shown that ENSO events of the past two decades can be skillfully predicted up to three seasons ahead (Barnston et al. 1999). The prediction performance of current CGCMs was found to be comparable to that of statistical models.

To achieve good prediction skills of ENSO requires a good coupled model and realistic initial conditions with a proper initialization procedure (e.g., Chen et al. 1997). Current state-of-the-art CGCMs still have difficulties in correctly simulating the climatology and ENSO variations in the tropical Pacific (e.g., Achutarao and Sperber 2002). Compared to observations, most CGCMs produce more frequent ENSO events with poor phase locking to the seasonal cycle and weaker ENSO amplitudes and teleconnections. The ill capture of air–sea interactions responsible for ENSO will deteriorate the prediction skill even with perfect initial conditions. Since the ENSO predictability mainly resides in the ocean memory (e.g., Neelin et al. 1998), a realistic oceanic condition could lead to a better prediction skill by assimilating subsurface observations into OGCMs (e.g., Ji and Leetmaa 1997; Rosati et al. 1997) or by adding the subsurface information as a predictor to statistical models (e.g., Smith et al. 1995; Clarke and van Gorder 2003). To generate good assimilation data for a particular OGCM, however, requires lots of efforts. Furthermore, due to the different physics used in different models, assimilation data with one OGCM cannot be directly applied to other OGCMs (Tang et al. 2003). Initial errors owing to the model physics mismatch could develop quickly to destroy the predictability in the presence of unstable air–sea interactions.

One classical and economical way to generate initial conditions is to force AGCMs with observed sea surface temperature (SST), and then vice versa, using the AGCM outputs to force OGCMs. Mismatch between the atmospheric and oceanic initial conditions, however, leads to an initial shock, reducing the forecast skill within the first several lead months. Many efforts have been made to generate consistent atmospheric and oceanic initial conditions using an iteration procedure (Kirtman et al. 1997), coupled nudging schemes (Chen et al. 1997; Rosati et al. 1997; Oberhuber et al. 1998), or anomaly initializations (Latif et al. 1994; Schneider et al. 1999). Recently, assimilation of both atmosphere and ocean observations into a coupled GCM is in progress (T. Awaji 2004, personal communication). By nudging observed wind stress into the simple coupled model, Chen et al. (1997) found that their model prediction skill is improved significantly. The SST-nudging scheme, however, degrades their model performance. The failure of both the wind- and SST-nudging schemes in the model of Rosati et al. (1997) is owing to too

diffusive thermocline produced by their OGCM. In the absence of atmospheric and oceanic assimilation data, success of the coupled nudging schemes is largely dependent on model performance in simulating the climatology and ENSO. Using the coupled SST-nudging scheme, Keenlyside et al. (2005) showed that their coupled model is able to predict ENSO at the 6-month lead time based on a nine-member ensemble hindcast experiment. The latest version of Cane–Zebiak model has also shown a skillful prediction over the 1-yr lead time based only on the SST-nudging initialization scheme (Chen et al. 2004). This is because that the model systematic biases have been statistically corrected (Chen et al. 2000; Barnett et al. 1993). In other words, the model physics has been better fitted to the observations.

Based on the European Union (EU)–Japan collaboration, we have developed a relatively high resolution ocean–atmosphere coupled GCM, named the Scale Interaction Experiment–Frontier Research Center for Global Change (FRCGC) (SINTEX-F) model (Luo et al. 2003). The ENSO variability is simulated realistically, including the magnitudes, period (3–5 yr), and meridional broadness of SST anomalies (Gualdi et al. 2003; Guilyardi et al. 2003; Luo et al. 2005). Such good performance of ENSO simulation is found to be related to the high-resolution (T106) of the atmosphere GCM (Guilyardi et al. 2004). One common bias that the cold tongue in the tropical Pacific extends too far west has also been reduced by improving the coupling physics (Luo et al. 2005). The dry bias in the western Pacific warm pool region is reduced. The ENSO signal in the equatorial western Pacific and the teleconnection in the North Pacific are simulated more realistically. In terms of the model good performance in simulating the climatology and ENSO in the tropical Pacific, we have implemented several hindcast experiments to check the model performance of ENSO prediction based on the simple coupled SST-nudging scheme for initialization. The coupled model, hindcast experiments, and initialization scheme are described in section 2. Model performance of ENSO prediction is presented in section 3. Predictabilities of climate signals in the tropical Indian Ocean and Atlantic are shown in section 4. A summary and discussion are given in section 5.

## 2. The coupled GCM and the hindcast experiments

### a. The SINTEX-F CGCM

The SINTEX-F coupled model was developed from the original European SINTEX model under the EU–Japan collaboration project (Gualdi et al. 2003; Guil-

yardi et al. 2003; Luo et al. 2003, 2005). The global ocean component is the reference version 8.2 of the Océan Parallélisé (OPA; Madec et al. 1998) with the ORCA2 configuration. To avoid the singularity at the North Pole, it has been transferred to two poles in the Eurasian and North American continent, respectively. The model longitude–latitude resolution is  $2^\circ \times 2^\circ \cos(\text{latitude})$  with increased meridional resolutions to  $0.5^\circ$  near the equator. It has 31 vertical  $z$  levels of which 19 lie in the top 400 m. Model physics includes a free-surface configuration (Roullet and Madec 2000) and the Gent and McWilliams (1990) scheme for isopycnal mixing. Horizontal eddy viscosity coefficient in open oceans varies from  $40000 \text{ m}^2 \text{ s}^{-1}$  in high latitudes to  $2000 \text{ m}^2 \text{ s}^{-1}$  in the equator. Vertical eddy diffusivity and viscosity coefficients are calculated from a 1.5-order turbulent closure scheme (Blanke and Delecluse 1993). Nonslip conditions are applied at lateral solid boundaries. The effect of solar radiation penetration under the sea surface is also included. [Readers are referred to Madec et al. (1998) or online at <http://www.lodyc.jussieu.fr/opa/> for more details.]

The atmosphere component is the latest version of ECHAM4 in which the Message Passing Interface is applied to parallel computation (Roeckner et al. 1996). We adopted a high horizontal resolution (T106) of about  $1.1^\circ \times 1.1^\circ$ . A hybrid sigma–pressure vertical coordinate is used with 4–5 of a total of 19 levels lying in the planetary boundary layer. Model physical processes include the Tiedtke (1989) bulk mass flux formula for cumulus convection and the Morcrette et al. (1986) radiation code. Cloud water and water vapor (tracers) are advected using the semi-Lagrangian scheme. Effects of gravity wave drag and cumulus friction are parameterized. Land surface processes are based on a five-layer model for soil temperature including the effects of soil hydrology and snowpack over land. The surface turbulent flux is calculated according to a bulk aerodynamic formula in which the drag coefficients for momentum and heat are estimated based on an approximate analytical function of the moist bulk Richardson number and roughness length (Louis 1979). Over the open water, the aerodynamic momentum roughness length is estimated from friction velocity (Charnock 1955). The original SINTEX coupled model with this high-resolution version is found to be able to improve the prediction of the development of intense ENSO episodes (Gualdi et al. 2005). We note that prediction skills of ENSO in their coarse-resolution (T42) model are rather low probably due to the biennial ENSO behavior.

The coupling fields (SST, surface momentum, heat and water fluxes, etc.) are interpolated and exchanged

every 2 h between the ocean and atmosphere by means of the Ocean Atmosphere Sea Ice Soil (OASIS 2.4) coupler (Valcke et al. 2000). The coupled model does not apply any flux correction except that sea ice cover is relaxed toward observed monthly climatologies in the OGCM. The initial condition of the atmosphere is provided by the 1-yr run forced with observed monthly climatological SST. The ocean is started from the Levitus annual mean climatologies with zero velocities.

#### *b. The hindcast experiments*

We have designed five hindcast experiments. Starting from the above initial conditions, the coupled model for each experiment has first been spun up for 11 yr in a decoupled mode. The two-hourly atmospheric outputs forced by Hadley Centre Global Sea Ice and Sea Surface Temperature (HadISST1.1; Rayner et al. 2003) for the period 1971–81 are used to spin up the ocean model in a synchronous manner. For the hindcast period 1982–2001, OGCM SSTs are strongly nudged toward the National Oceanic and Atmospheric Administration/Climate Diagnostics Center (NOAA/CDC) SST observations (Reynolds et al. 2002) in a coupled mode. Weekly NOAA/CDC SSTs have been interpolated into daily mean using a cubic spline method. A large negative feedback value ( $-2400 \text{ W m}^{-2} \text{ K}^{-1}$ ) to the surface heat flux is applied. This value corresponds to the 1-day relaxation time for temperature in the 50-m mixed layer. The AGCM forced by such generated OGCM SSTs, which are very close to the observations, tends to produce realistic wind stress, heat, and water fluxes (see Fig. 2 in section 3a). The OGCM forced by the AGCM wind stress in turn tends to produce realistic thermocline variations in the equatorial Pacific. Thus, the success of the simple coupled SST-nudging scheme for initialization crucially depends on the performance of both AGCMs and OGCMs.

Surface wind stress is important for the tropical air–sea coupling system. Large uncertainties, however, exist in the wind stress estimations. To generate the five hindcast ensemble members, we have perturbed the coupling physics for each member separately. In the first seasonal forecast experiment (SFE1), the effects of ocean surface current on wind stress are neglected as is done in most existing CGCMs. In terms of the importance of the strong surface current in the equatorial Pacific, surface current momentum is directly passed to the atmosphere in the second experiment (SFE2). This affects both wind stress and heat flux calculations. The external momentum source further influences the global angular momentum budget of the atmosphere (Luo et al. 2005). The ocean surface is kept solid relative to the atmosphere in the third one (SFE3), but the surface

wind stress (only) is calculated by  $\tau = \rho_a C_D |\mathbf{v}_a - \mathbf{v}_o| (\mathbf{v}_a - \mathbf{v}_o)$  (see also Pacanowski 1987). Here  $\rho_a$  is the density of air,  $C_D$  is the drag coefficient,  $\mathbf{v}_a$  is the wind velocity at the lowest level of the AGCM, and  $\mathbf{v}_o$  is the ocean surface velocity at a 5-m depth (the uppermost layer of the OGCM). The coupling physics in the last two experiments (SFE4 and SFE5) is the same as that in SFE2 and SFE3 except that ocean surface velocities are partly dropped from the bulk formula. That is, we set  $\tau = \rho_a C_D |\mathbf{v}_a| (\mathbf{v}_a - \mathbf{v}_o)$ . Readers are referred to Luo et al. (2005) for more details. We note that, as practical methods, SFE4 and SFE5 do account for some uncertainties in the wind stress estimation as shown in sections 3 and 4.

The classical ensemble method for a single CGCM is to perturb the initial conditions of atmosphere and/or ocean whose physics is kept unchanged. Recent results have shown that ensemble forecasts based on multi-independent models are able to significantly improve both deterministic and probabilistic prediction skills (e.g., Krishnamurti et al. 1999; Palmer et al. 2004). This is mainly because of the error cancellation among different models (Hagedorn et al. 2005). The perturbed coupling physics tends to modify model climatologies in the equatorial Pacific (Luo et al. 2005). This could affect the climate drift during forecasts. Furthermore, the ocean surface current may modify the actual driving force of the westerly (easterly) wind bursts. This could influence the evolution of individual ENSO event as shown by Fedorov et al. (2003). The ensemble approach used in this study lies between the classical and the multimodel one. It tries to account for the uncertainties associated with not only the initial conditions but also the model physics. The models with merely modified coupling physics, however, are not largely independent. Similar biases among them could not be canceled by a simple ensemble mean without posterior model calibrations (Doblas-Reyes et al. 2005, and references therein). We note that a similar idea is to use multiple or stochastic-dynamic parameterizations for a given subgrid process based on a single GCM (e.g., Palmer 2001). This has been found to improve weather and climate predictability. In this study, for the sake of simplicity, we have adopted the simple ensemble mean method and measured deterministic prediction skills. This provides a lower bound of ENSO predictability of the SINTEX-F model.

### 3. Results

#### a. Initial conditions

Figure 1 shows 20°C isotherm depth anomalies along the equatorial Pacific (2°S–2°N) from both the Simple

Ocean Data Assimilation (SODA; Carton et al. 2000) and model results. The latter is a simple average of the five ensemble members. The anomaly fields of each ensemble member have been calculated separately based on its own climatology for the period 1983–2001. Compared to the SODA observations, the model realistically captures the thermocline variations associated with the interannual ENSO events in the past 20 yr. The eastward-propagation features along the equator are well simulated. The intermittent warm signals in the early 1990s are also captured. Amplitudes of the thermocline fluctuations are comparable to the SODA reanalysis. The results indicate that the SINTEX-F coupled model is able to generate realistic oceanic memory for the ENSO prediction using the simple SST-nudging scheme.

The good simulation of the subsurface signal in the equatorial Pacific is related to the realistic wind stress forcing produced by the AGCM (Fig. 2). Low-frequency westerly (easterly) anomalies related with the El Niño (La Niña) events are well captured. The eastward propagations of the anomalous westerlies associated with the strong 1982/83 and 1997/98 warm episodes are simulated. Furthermore, the AGCM is able to capture some intraseasonal westerly (easterly) wind bursts in the western equatorial Pacific (see arrows in Fig. 2a). The westerly wind bursts in the early 1990s and during the onset phase of the 1997/98 El Niño episode are captured realistically. The simulated magnitudes, however, are generally smaller than the SODA analysis. We note that the rather noisy structure of the SODA wind stress before 1986 is due to the lack of the Tropical Atmosphere Ocean (TAO) observations.

Based on the generally realistic initial conditions, we have implemented the 12-month forecast with the freely coupled GCM starting from 0000 UTC on the first day of each month of each year from 1982 to 2001. The restart files for each ensemble member forecast at each time is obtained from the instantaneous state at the same time generated by the coupled SST-nudging run with the perturbed coupling physics as described in section 2b.

#### b. Model drift

Because of model deficiencies, the climate state inevitably drifts toward the model's own climatology once the forecast starts. How large the drift is depends on the prediction lead time, errors in initial conditions, and model physics. Here, we define the lead time as the length of forecast integrations. For example, 1-month lead prediction refers to the monthly mean of the first

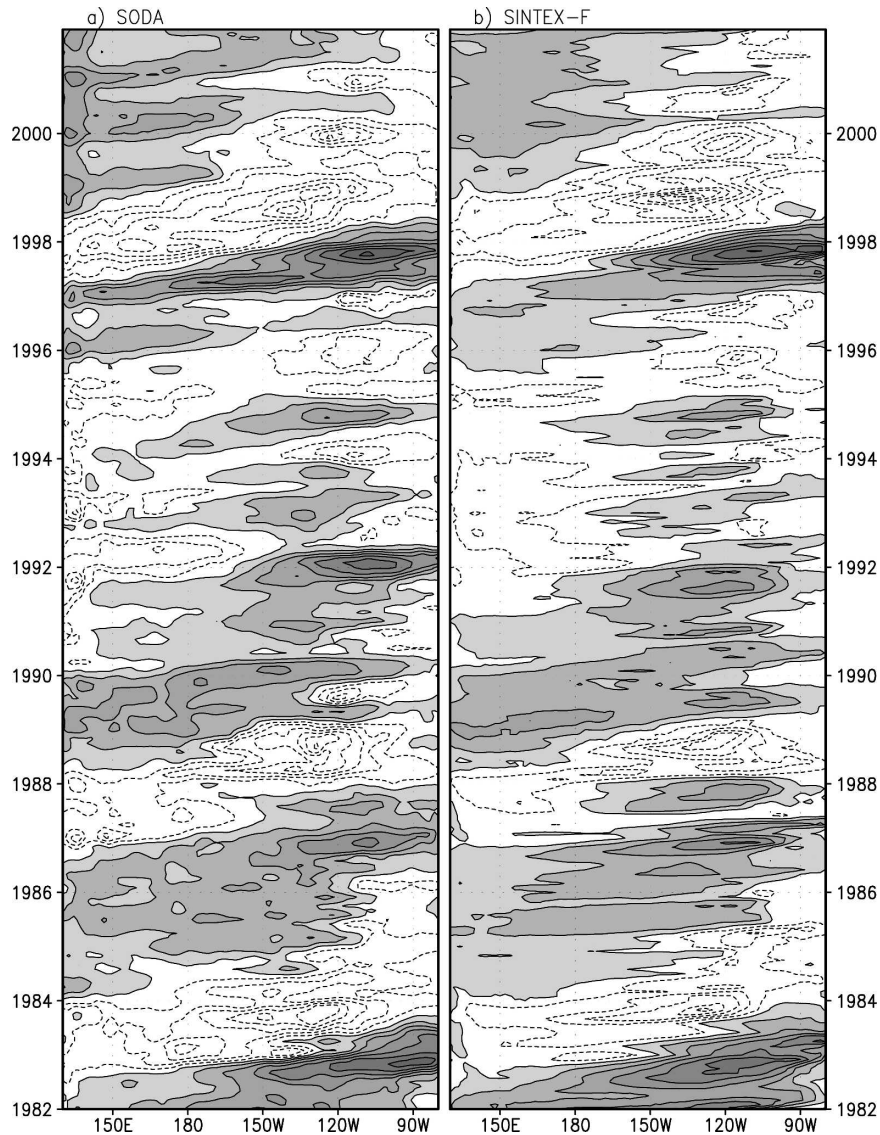


FIG. 1. The 20°C isotherm depth anomalies (contour: 10 m) along the equatorial Pacific (2°S–2°N) from (a) SODA and (b) model results based on the SST-nudging scheme. Regions with positive values are shaded.

month integrations from the initial condition. Figure 3 shows annual mean climatologies of the predicted equatorial SST at 1- and 12-month lead times. SST in the eastern equatorial Pacific immediately shifts to a colder state (Fig. 3a). This is caused by the mean thermocline there, which is too shallow in initial conditions (not shown), probably forced by too strong a surface easterly wind along the equator (see Luo et al. 2005). This problem could be solved by subsurface data assimilation in the future. SST at 120°W is up to 1.2°–1.6°C colder than the observation after the 3-month free integrations, and then it gradually warms up, slowly approaching the model's own climatology there

(Luo et al. 2005). The cold SST bias in the eastern Pacific gradually extends westward and leads to a colder state in the central and western part (Fig. 3b). The cold bias in the latter region, however, is reduced by taking ocean surface current into account for wind stress calculation in various ways. In particular, the cold SST bias there is much smaller in SFE2 and SFE4 in which surface current momentum is directly passed to the atmosphere (see thin solid and dotted lines in Fig. 3b). The equatorial zonal SST gradients, as determined by the air–sea interactions (e.g., Dijkstra and Neelin 1995), are also closer to observations with the improved coupling physics. This is consistent with the 100-yr sen-

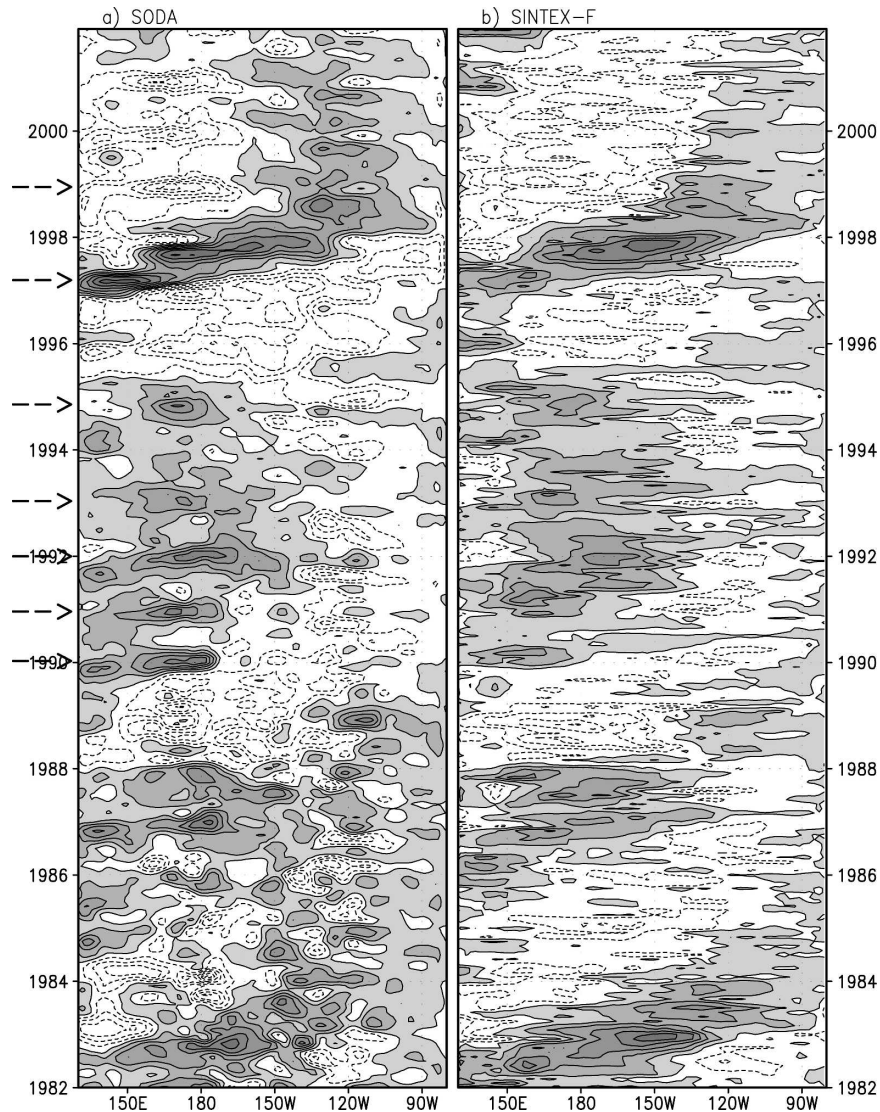


FIG. 2. Same as in Fig. 1, but for the zonal wind stress anomalies (contour:  $0.1 \text{ dyn cm}^{-2}$ ). Values in (a) have been spatially smoothed with nearby 9 points to filter out the noisy structure of SODA analysis. Thick arrows denote the intraseasonal signals captured by the model.

sitivity experiment results of Luo et al. (2005). The SST bias in the equatorial Indian Ocean is rather small within the first 12-month forecasts. SST in the eastern Atlantic, however, continuously warms up; zonal SST gradients in the central Atlantic are reversed after the 12-month free integrations. This is similar to the intrinsic bias in the coupled model climatology there (Luo et al. 2005).

Following the conventional approach, climate drifts based on different seasons and lead times are removed for each ensemble member (e.g., Kirtman et al. 1997; Stockdale 1997). Anomaly fields of the five members are then simply averaged to get the ensemble mean

forecasts. Since we focus on the predictability of climate changes beyond the intraseasonal time scale, observations and ensemble mean forecasts at each lead time have been smoothed with the 5-month running mean prior to the anomaly correlation coefficient (ACC) and root-mean-square error (rmse) calculations. This tends to give proper estimates of the climate predictability of the model when we substantially increase the ensemble members in the real-time forecasts. We note that in the Indian Ocean, where the intraseasonal oscillations are strong and active, five ensemble members are far too small to estimate the influence of the intraseasonal signals.

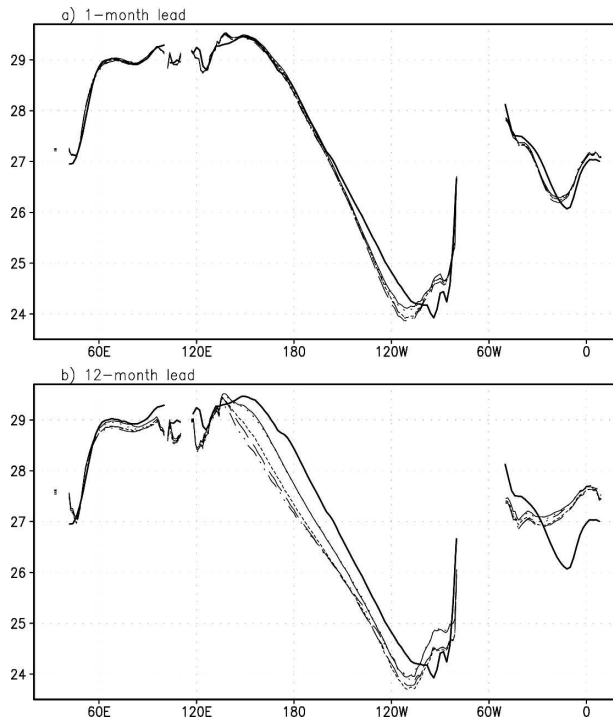


FIG. 3. SST climatology of the period 1983–2001 along the equator ( $2^{\circ}\text{S}$ – $2^{\circ}\text{N}$ ) based on the NOAA/CDC observations (thick solid lines), SFE1 (dot-dot-dashed lines), SFE2 (thin solid lines), SFE3 (short dashed lines), SFE4 (dotted lines), and SFE5 (long dashed lines) for the (a) 1- and (b) 12-month lead time forecasts.

### c. ENSO predictability

Figure 4 shows the ACC skill scores of global SST predictions at 3-, 6-, 9-, and 12-month lead times for the period 1982–2001. The model produces useful skill ( $\geq 0.6$ ) of SST predictions in most of Pacific and tropical Indian and Atlantic Oceans at the 3-month lead time (Fig. 4a). The highest predictability appears in the central and eastern equatorial Pacific associated with the interannual ENSO events as expected. The ACC in this region reaches above 0.9 at the 3-month lead time, and then gradually decrease to about 0.8, 0.7, and 0.6 at 6-, 9-, and 12-month lead times, respectively (Figs. 4a–d). We note that ACC skills of ENSO based on unfiltered forecasts and observations are only about 0.1 lower because of its predominant interannual variations. The ENSO teleconnections in the North and South Pacific also show considerable predictabilities until the 9-month lead time. Besides, significant SST predictabilities are found in the tropical North Atlantic and western and eastern tropical South Indian Ocean. Results of those two basins will be described in section 4.

The interannual ENSO events are able to be predicted by the model up to the 1-yr lead time (Fig. 5a). Both the El Niño events in 1982/83, 1986/87, 1991/92,

and 1997/98 and the La Niña events in 1984/85, 1988/89, and 1999/2000 are successfully predicted. Prediction of the strongest 1997/98 warm event was found to be very difficult and failed by most existing CGCMs beyond the 6-month lead time (e.g., Barnston et al. 1999; Landsea and Knaff 2000). The SINTEX-F model is capable to predict this unprecedented event at the 9-month lead time with an amplitude as large as  $2.2^{\circ}\text{C}$ . At the 12-month lead time, however, the predicted signal is only about  $1.3^{\circ}\text{C}$ , about one-half of the observations. For the weak warm signals in 1992/93 and 1994/95, the model also shows considerable predictabilities at the 6–9-month lead times. For the 1991/92 El Niño event, the model predicted an earlier than observed peak and a weaker magnitude at the short (3 month) lead time. This is due to the similar errors in initial conditions (Fig. 1). Similarly, the overestimated 1999/2000 La Niña event at the short lead prediction seems to be related to a cold bias in initial conditions. Better initial conditions with data assimilation may improve the forecasts (e.g., Ji and Leetmaa 1997). During the period 1982–2001, there is only one false alarm of a weak warm event in 1990/91. We note that the model tends to correctly predict the El Niño event in 2002/03.

Compared to the persistence forecast, model predictions of the Niño-3.4 SST index show much higher ACC skills not only at long (9 months and beyond) lead times but also at short lead times (Fig. 5b). The ensemble mean forecast skill is above 0.7 at the 12-month lead time (solid line in Fig. 5b). We note that the skill based on the unfiltered data is still above 0.6 at the 12-month lead time. The initial shock is largely reduced using the compatible initial conditions between the atmosphere and ocean as generated by the coupled SST-nudging scheme. The model rmses at mid (6 month) and long lead times are less than 50% of the persistence and much smaller than one standard deviation of  $0.97^{\circ}\text{C}$  (Fig. 5c). We note that the different systematic SST biases from each ensemble member in the equatorial Pacific do not lead to significant differences in the ENSO prediction skills (see short dashed lines in Figs. 5b,c). This is probably related to the fact that the climate drifts of each member (not largely different) have been removed in a posterior manner.

The low-frequency variations of the equatorial thermocline and zonal wind can be predicted at long lead times. The eastward propagations of subsurface signals along the equatorial Pacific are successfully predicted at the 12-month lead time (Fig. 6a). This suggests a potential predictability of ENSO beyond the 1-yr lead time. The predicted magnitudes of the equatorial thermocline variations, however, gradually decrease as the lead time increases. This is consistent with the weak-

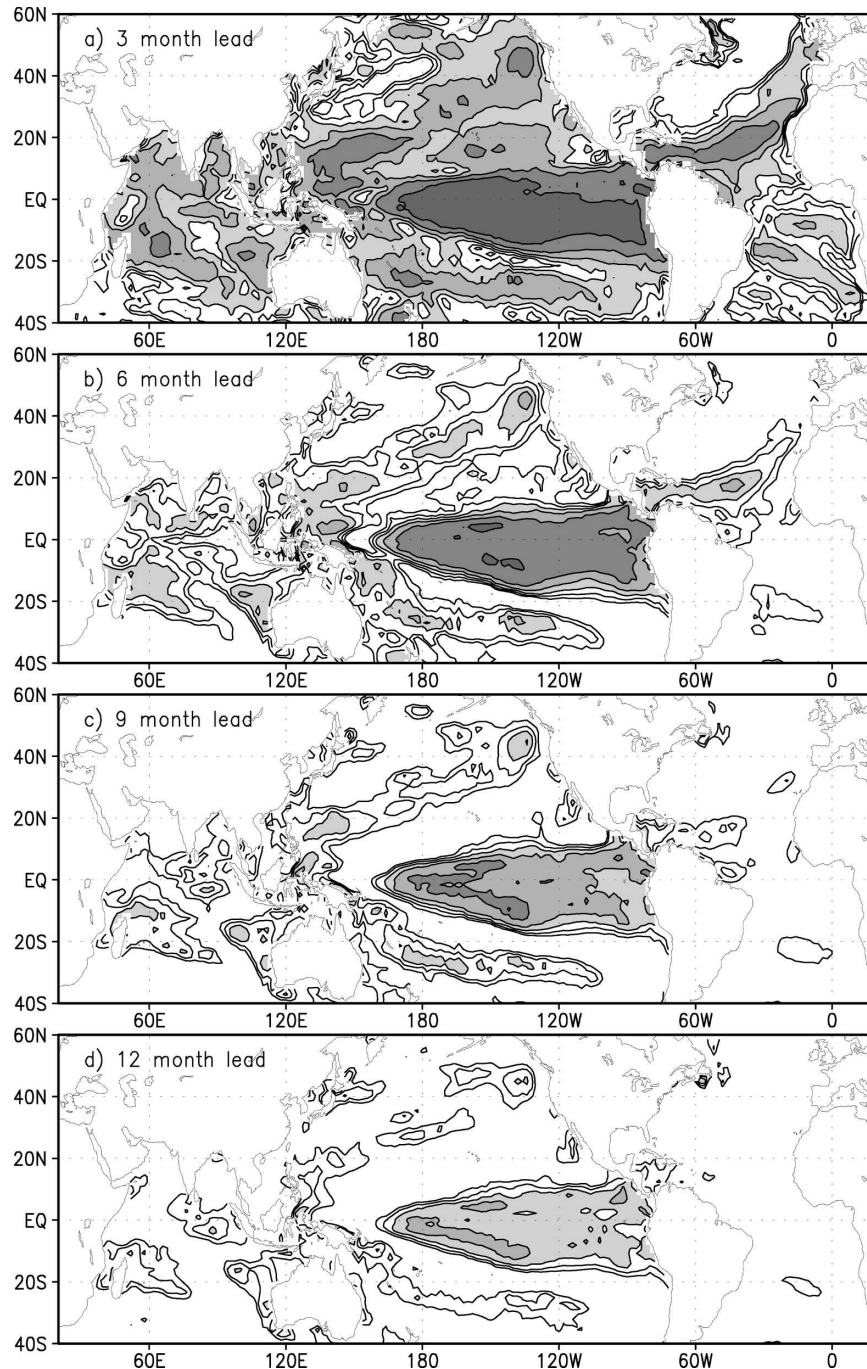


FIG. 4. (a)–(d) Model ACC skill scores of global SST predictions at 3-, 6-, 9-, and 12-month lead times. Contour interval is 0.1 and regions with values above 0.6 are shaded.

ened amplitudes of the predicted Niño-3.4 SST anomalies at long lead times, in particular, during the 1988/89 La Niña and 1997/98 El Niño events (see Fig. 5a). The predicted peak phases of these two events are clearly delayed as the lead time increases. To understand the possible reasons, we have plotted in Fig. 6b the zonal

wind stress anomalies in the western equatorial Pacific ( $2^{\circ}\text{S}$ – $2^{\circ}\text{N}$ ,  $150^{\circ}\text{E}$ – $180^{\circ}$ ). The SODA analysis shows two easterly wind bursts in 1988 and two strong westerly wind ones in 1997 (see the long dashed line in Fig. 6b). At a few months lead, the wind bursts can be predicted but with weaker values (see the solid line in Fig. 6b). At

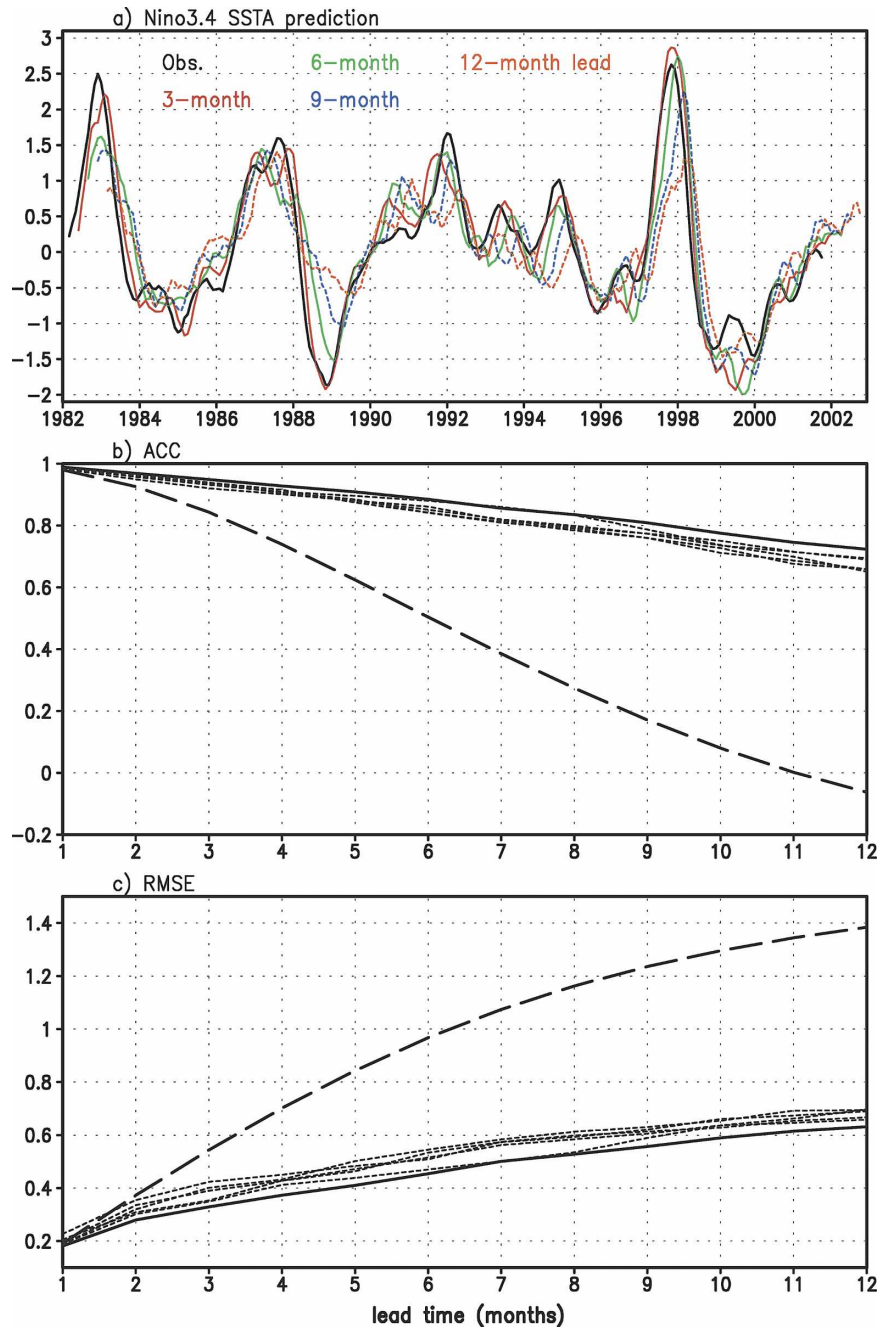


FIG. 5. (a) Niño-3.4 SSTA anomalies ( $5^{\circ}\text{S}$ – $5^{\circ}\text{N}$ ,  $170^{\circ}$ – $120^{\circ}\text{W}$ ) based on the NOAA/CDC observations (solid line) and model predictions at 3- (red line), 6- (green line), 9- (blue line), and 12-month (yellow line) lead times. Results have been smoothed with 5-month running mean. (b), (c) ACC scores and rmses of the persistence (long dashed lines), ensemble mean (solid lines), and individual member forecasts (short dashed lines).

mid and long lead times, however, the model shows no predictability of these intraseasonal signals (see the short dashed line in Fig. 6b). Similar behaviors also appear for the three weak warm episodes in the early 1990s when the westerly wind bursts are active (Figs. 5a

and 6b). This is consistent with some existing studies showing that the intraseasonal wind bursts in the western equatorial Pacific may trigger and amplify the ENSO events under some circumstances (McPhaden 1999; Fedorov et al. 2003; Lengaigne et al. 2004). In

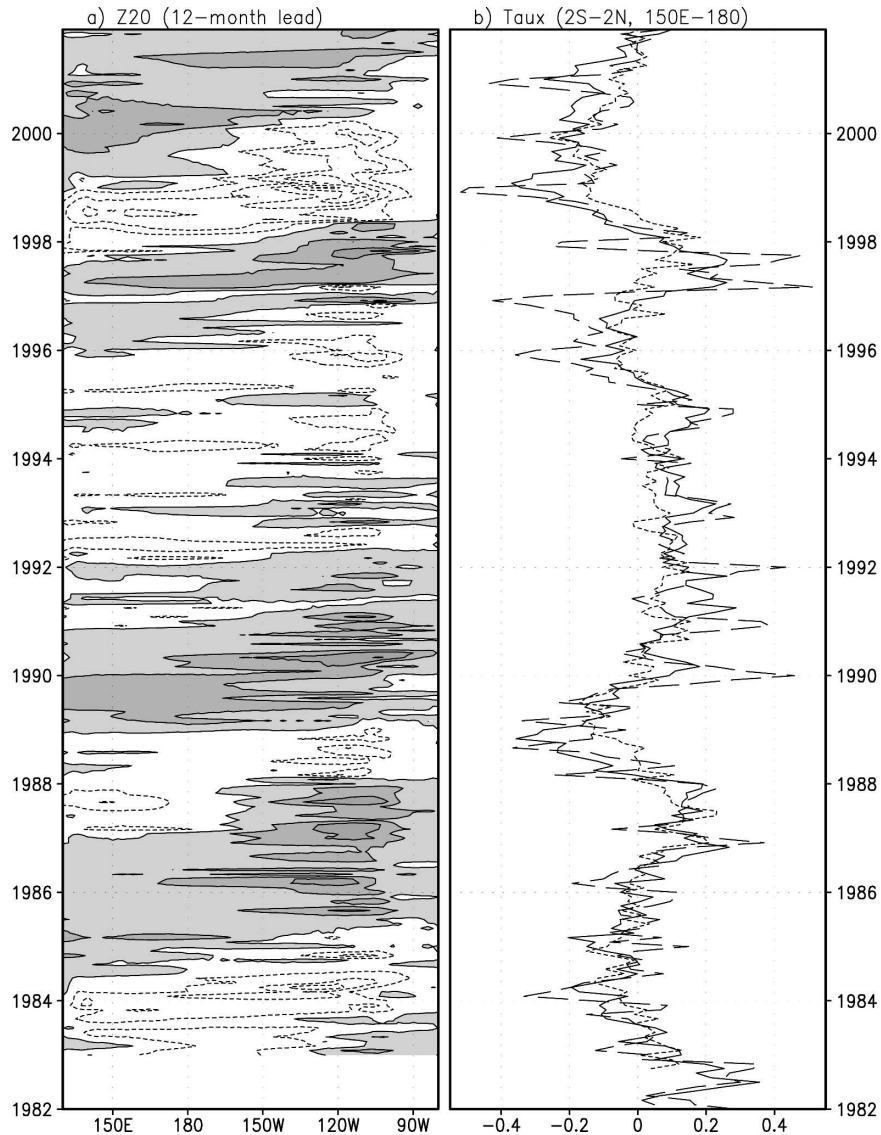


FIG. 6. (a) Same as in Fig. 1b, but for the 20°C isotherm depth anomalies predicted at the 12-month lead time. (b) Zonal surface wind stress anomalies in the western equatorial Pacific (2°S–2°N, 150°E–180°) from the SODA analysis (long dashed line), and the predictions at 1- (solid line) and 9-month (short dashed line) lead times. We note that the time series of the 1-month lead time forecasts is similar to that produced by the SST-nudging initialization (see Fig. 2b) but with weakened magnitudes.

other cases, for example, during the 1984/85 and 1999/2000 cold and 1986/87 warm events, when the wind bursts are weak or have no significant impacts, the model is able to predict the ENSO events very well at long lead times (Fig. 5a). The long lead-predicted subsurface signals in these cases also do not weaken too much (see Figs. 1b and 6a).

#### d. The spring prediction barrier

Observations and existing model predictions have shown that ENSO persistence and predictability de-

crease rapidly during springtime (e.g., Webster and Yang 1992; Latif et al. 1994). One of possible reasons is the phase locking of ENSO to the seasonal cycle; the phase transition of ENSO in spring leads to a low signal-to-noise ratio (e.g., Rasmusson and Carpenter 1982; Xu et al. 1994). We note that the SINTEX-F CGCM captures the seasonal phase locking of ENSO (Tozuka et al. 2005). As expected, the intrinsic “spring prediction barrier” appears in the model forecasts (Fig. 7a). The model prediction skills decrease rapidly in spring, reach minima in summer, and then slightly rebound in

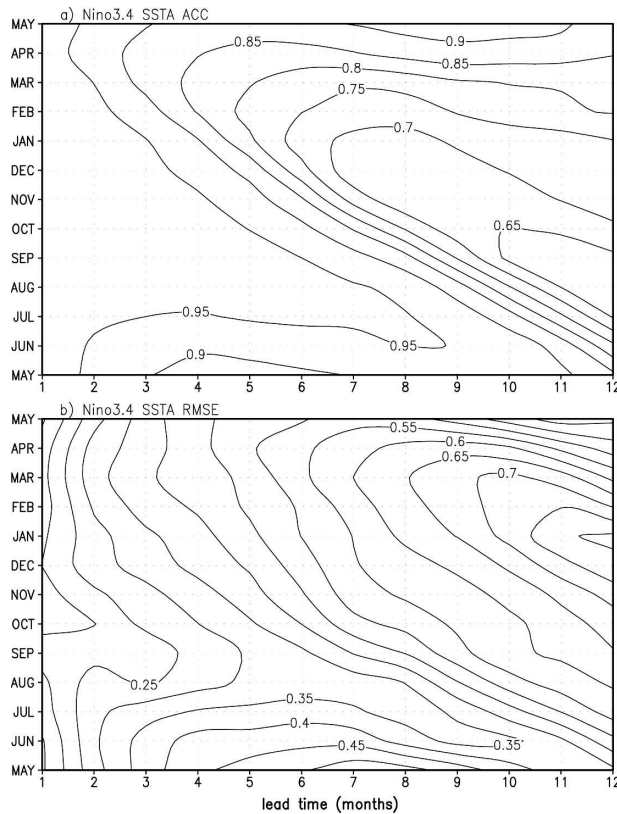


FIG. 7. Seasonally stratified ACC scores and rmse of the Niño-3.4 SST anomaly predictions.

fall. The prediction skills starting from each month, however, still reach above 0.6 at the 12-month lead time. In particular, predictions starting from 1 April and 1 May show ACC skills as high as 0.85 even at the 1-yr lead time. Rmse of the model predictions starting from each month show a rapid increase during spring associated with the “spring barrier” (Fig. 7b). However, maximum rmse appear in fall rather than in summer. This is related to the pronounced semiannual signal of SST in the eastern equatorial Pacific due to the model deficiencies (Luo et al. 2005): Warm SST peaks appear in both spring and fall. Such a semiannual cycle also appears in the short and long lead time predictions (not shown). The false warm SST peak in the east in fall slackens the zonal SST gradients along the equatorial Pacific. Thus, model errors could be amplified due to the incorrect air–sea interactions in fall.

#### e. Global predictabilities during different ENSO phases

Coupled models have difficulties in producing and predicting the meridional broad structure of ENSO SST anomalies and teleconnections in the extratropics

(e.g., Barnett et al. 1993; Kirtman et al. 1997; Davey et al. 2002). Figure 8 shows the spatial patterns of both observed and predicted typical ENSO SST anomalies during the peak phase, as calculated by one-half the differences between three El Niño events (1986/87, 1991/92, and 1997/98) and three La Niña events (1984/85, 1988/89, and 1999/2000). At the short lead time, the model predicts ENSO magnitudes as strong as the observations with realistic meridional broadness in the tropical Pacific (Figs. 8a,b). The cold SST anomalies in the central North and South Pacific, the warm anomalies along the eastern boundary in the North Pacific, the basinwide warm signals in the tropical Indian Ocean and the cold anomalies near the western coast of Australia are well predicted. At 6- and 9-month lead times, the meridional broadness of SST anomalies and the ENSO teleconnections in the North and South Pacific and Indian Ocean are successfully predicted (Figs. 8c,d). The predicted ENSO magnitudes in the equatorial Pacific, however, weaken slightly. The 12-month lead time predictions also show a similar pattern of SST anomalies but with much weaker magnitudes (not shown). This is related to the fact that some of long lead–predicted ENSO events are much weaker and delayed in the phase (see Fig. 5a).

Figure 9 shows the observed and predicted global precipitation anomalies during the peak phase of ENSO at 3-, 6-, and 9-month lead times. Associated with El Niño events, for example, more rainfall appears in the central and eastern equatorial Pacific, and less rainfall does in the intertropical convergence zone (ITCZ) and the South Pacific convergence zone (SPCZ; Fig. 9a). In the tropical Indian Ocean, less (more) rainfall is observed in the eastern (western) region. These precipitation changes are successfully predicted by the model at 3-, 6-, and 9-month lead times (Figs. 9b–d). Besides, the drought in the northeastern Brazil associated with the zonal Walker cell changes and the flood near the eastern boundary in the North Pacific and near the western coast of the southeastern America associated with the Pacific–North American (PNA) teleconnection are also well predicted. We note that the model predictions show a systematic flood bias over Indonesia at all three lead times. Whether it is due to the insufficient resolution or deficiencies in model physics requires further study.

SST anomalies during the developing phase of ENSO [June–July–August (JJA+0)] are predicted realistically (Fig. 10). In the summer when ENSO is growing, significant SST anomalies confined along the equatorial Pacific have already appeared (Fig. 10a). Both the equator-confined structure and magnitudes are predicted correctly at the 3-month lead time (Fig. 10b). At

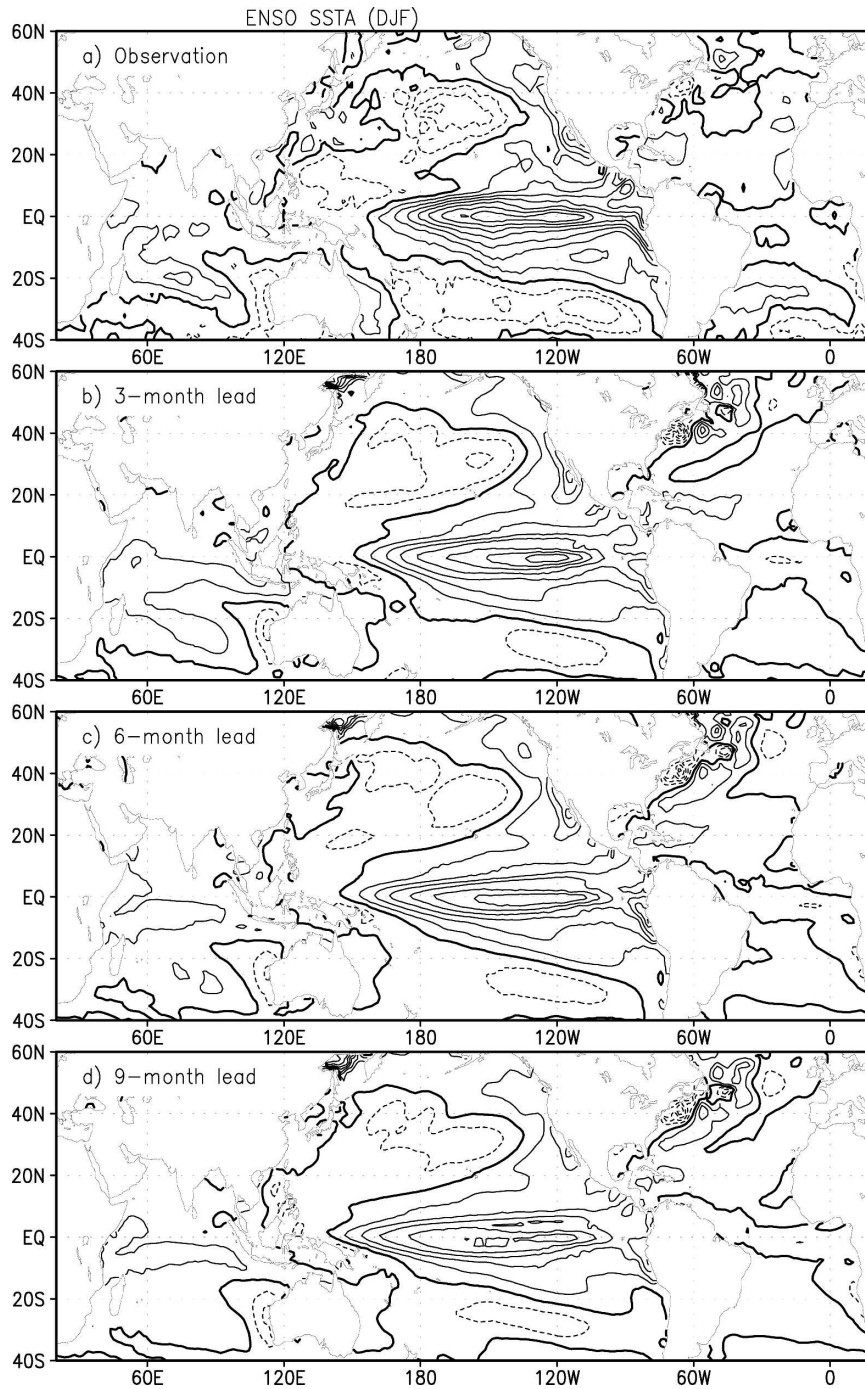


FIG. 8. SST anomaly differences in winter (from Dec to Feb) between the 1986/87, 1991/92, and 1997/98 El Niño events and the 1984/85, 1988/89, and 1999/2000 La Niña events based on (a) the observations and (b) 3-, (c) 6-, and (d) 9-month lead time predictions. Results have been divided by 2 in order to show the typical ENSO magnitudes. Contour interval is  $0.3^{\circ}\text{C}$  and thick solid lines denote zero contours.

6- and 9-month lead times, the equator-confined structure is predicted successfully but with much weakened magnitudes (Figs. 10c,d). This is related to the fact that some ENSO onsets are delayed in the model predic-

tions (see Fig. 5a). The warm SST anomalies in the developing phase induce more rainfall in the central equatorial Pacific and north of equator in the east, and less rainfall in the eastern equatorial Indian Ocean, In-

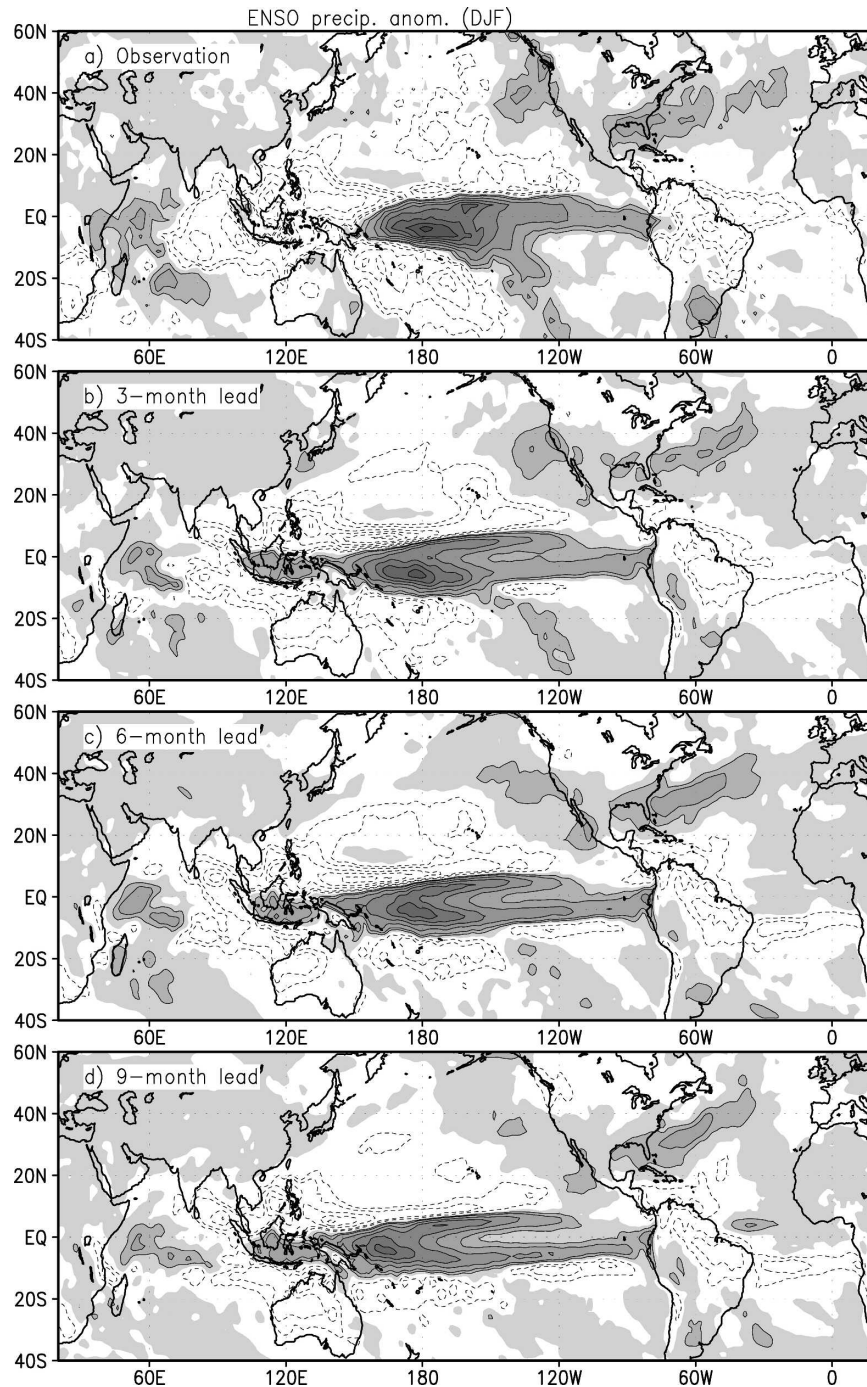


FIG. 9. Same as in Fig. 8, but for the global precipitation anomalies (contour:  $\pm 0.5$ ,  $\pm 1$ ,  $\pm 2$ ,  $\pm 3 \text{ mm day}^{-1}$  . . .). The observations are obtained from the Xie–Arkin (1996) analysis. Regions with positive values are shaded.

onesia, the SPCZ, the Caribbean area, and the north equatorial Atlantic (Fig. 11a). These precipitation changes are predicted at both short and long lead times (Figs. 11b–d). The negative correlation between the Indian summer monsoon rainfall and ENSO has signifi-

cantly weakened during the last decades (Kumar et al. 1999). Indeed, observations show slight good summer monsoons in the El Niño years during the past two decades (Fig. 11a). The model, however, predicts a significant drought in India at the short lead times

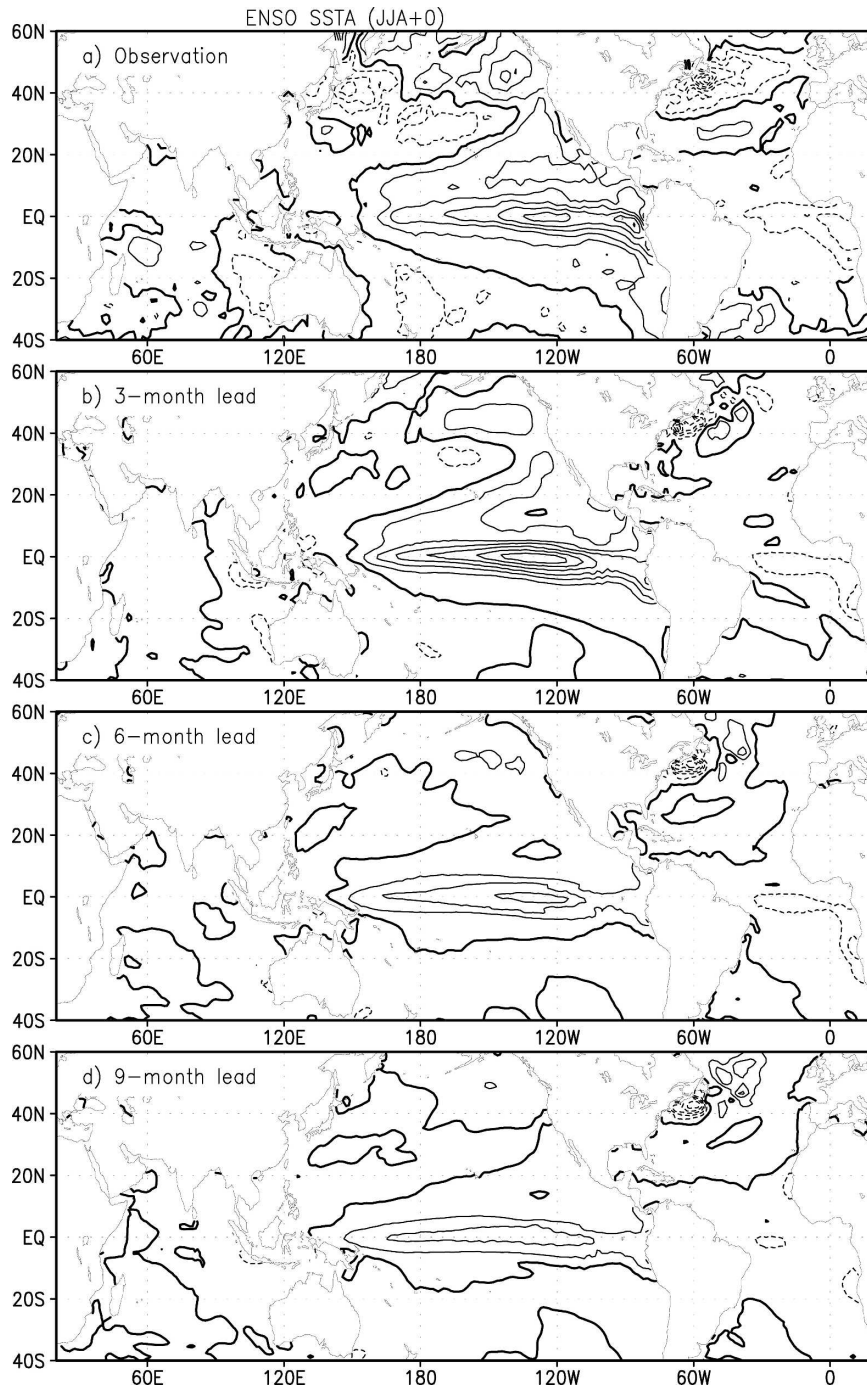


FIG. 10. Same as in Fig. 8, but for the global SST anomalies in summer (from Jul to Aug) prior to the ENSO peak phase.

(Fig. 11b). In particular, a severe drought summer in India is predicted in 1997 by the model at both short and long lead times (not shown).

In the following summer after the ENSO year (JJA+1), SST anomalies in the central and eastern tropical Pacific become rather weak (Fig. 12a). Cold

anomalies start to appear in the equator. The weak but meridionally broad SST anomalies are well predicted at both short and long lead times (Figs. 12b–d). The zonally elongated cold anomalies in the North Pacific at about 40°N are predicted amazingly well. The basin-wide weak warm SST anomalies in the tropical Indian

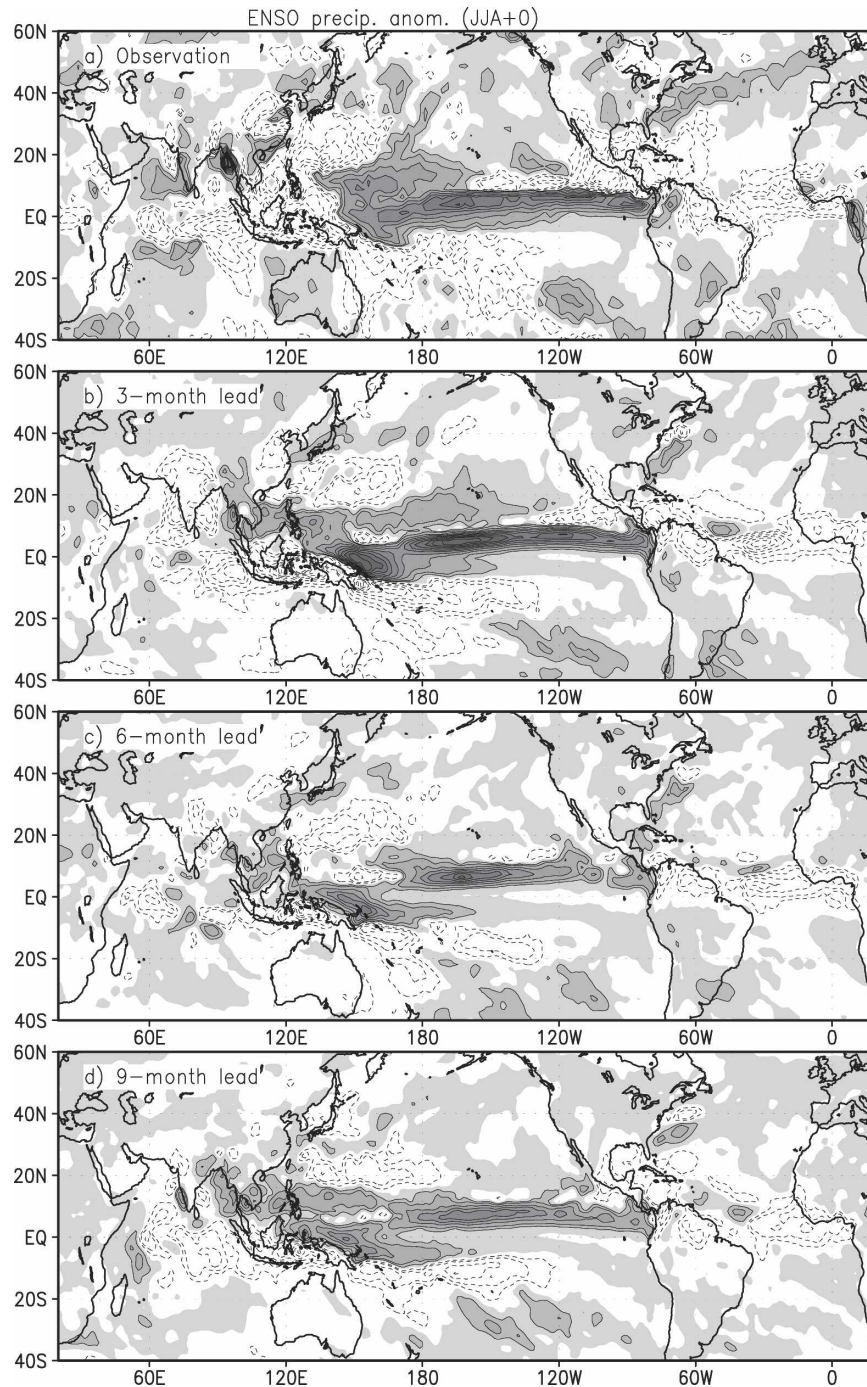


FIG. 11. Same as in Fig. 10, but for the precipitation anomalies (contour:  $\pm 0.25$ ,  $\pm 0.5$ ,  $\pm 1$ ,  $\pm 1.5$  mm day $^{-1}$  ...).

Ocean are predicted. Precipitation changes in the following summer after warm ENSO events show less rainfall in the SPCZ, ITCZ, and in Indonesia (Fig. 13a). More rainfall appears north of the equator in the eastern Pacific and south of the equator in the central region, which extends southeastward. In the equatorial

Indian Ocean, more summer rainfall appears after the El Niño events. Those signals are successfully predicted at both short and long lead times (Figs. 13b–d). The flood near the western coast of India, however, is not captured by the model. In east Asia, less rainfall appears in the south (east of the Philippines) and more

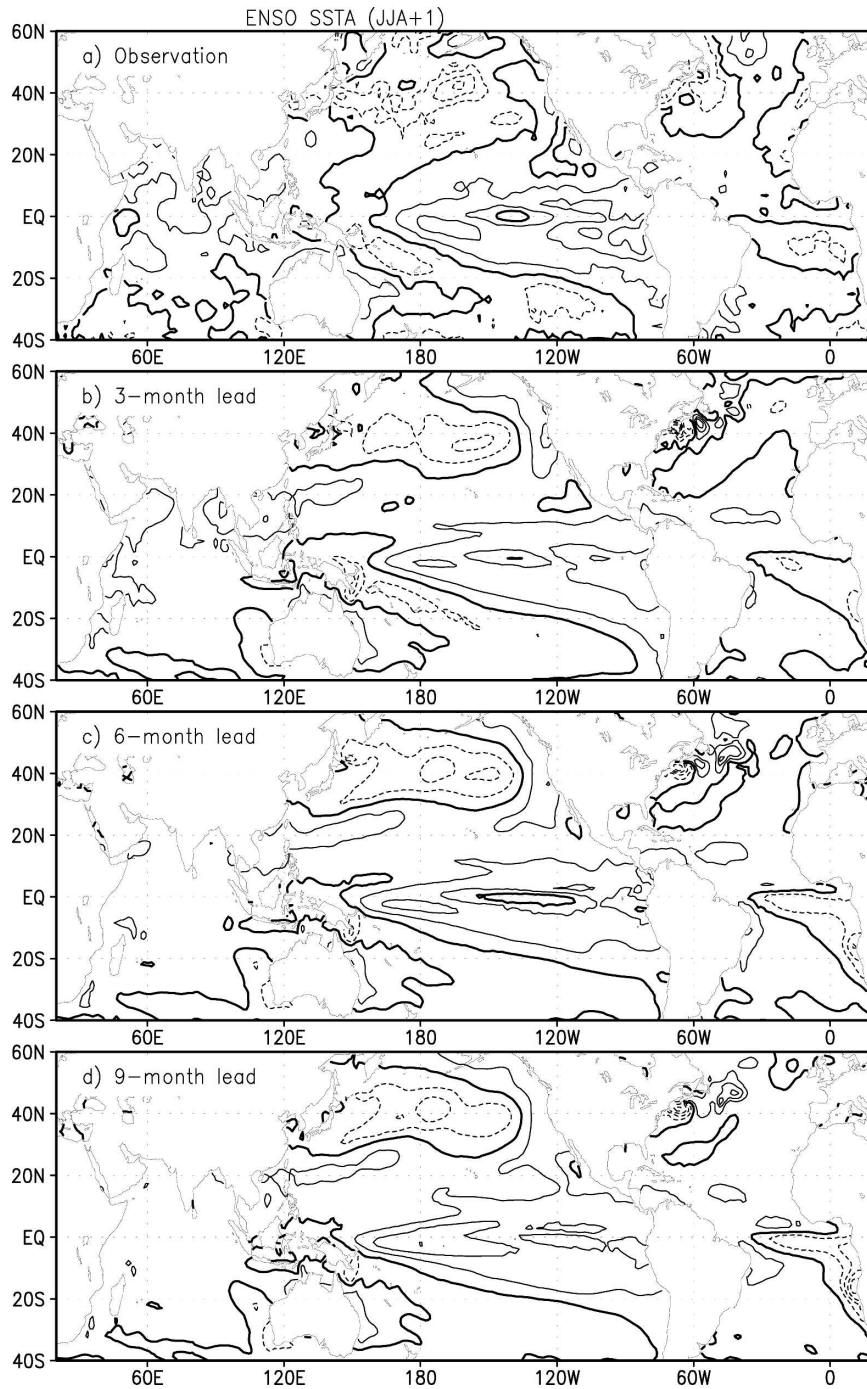


FIG. 12. Same as in Fig. 8, but for the global SST anomalies in the following summer (from Jul to Aug) after the ENSO peak phase.

rainfall appears in the north (near Japan). This is associated with the east Asian summer monsoon system. They are successfully predicted at both short and long lead times. Precipitation changes in the tropical Atlantic and the flood in the southeastern Brazil are also

predicted. However, the model tends to produce more rainfall north of the South China Sea and north of Indonesia; this is opposite to the observations. The summer global drought/flood signals after ENSO are also predicted at the 12-month lead time (not shown).

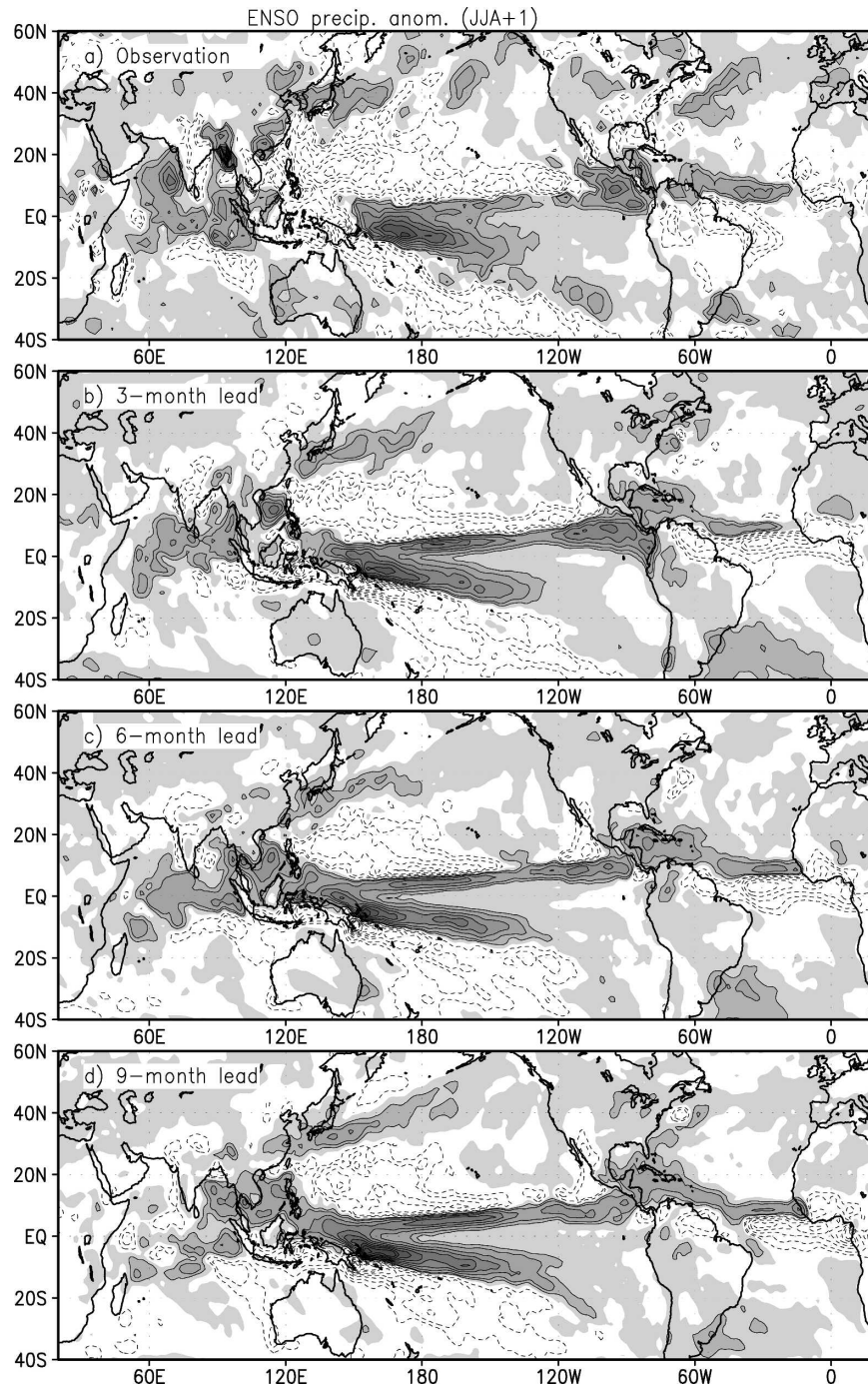


FIG. 13. Same as in Fig. 12, but for the precipitation anomalies (contour:  $\pm 0.25$ ,  $\pm 0.5$ ,  $\pm 1$ ,  $\pm 1.5$  mm day $^{-1}$  ...).

#### 4. Predictabilities in the tropical Atlantic and Indian Oceans

The interannual climate variations in the tropical Atlantic and Indian Oceans are affected by both the remote influence of ENSO and local air–sea interactions.

The climate signals in these two basins are rather weak compared to ENSO. Therefore, to enhance seasonal predictabilities in these two basins is a challenge (see Fig. 4). In particular, to predict interannual variations due to local air–sea interactions in the equatorial Atlantic and Indian Ocean is not easy even at short lead

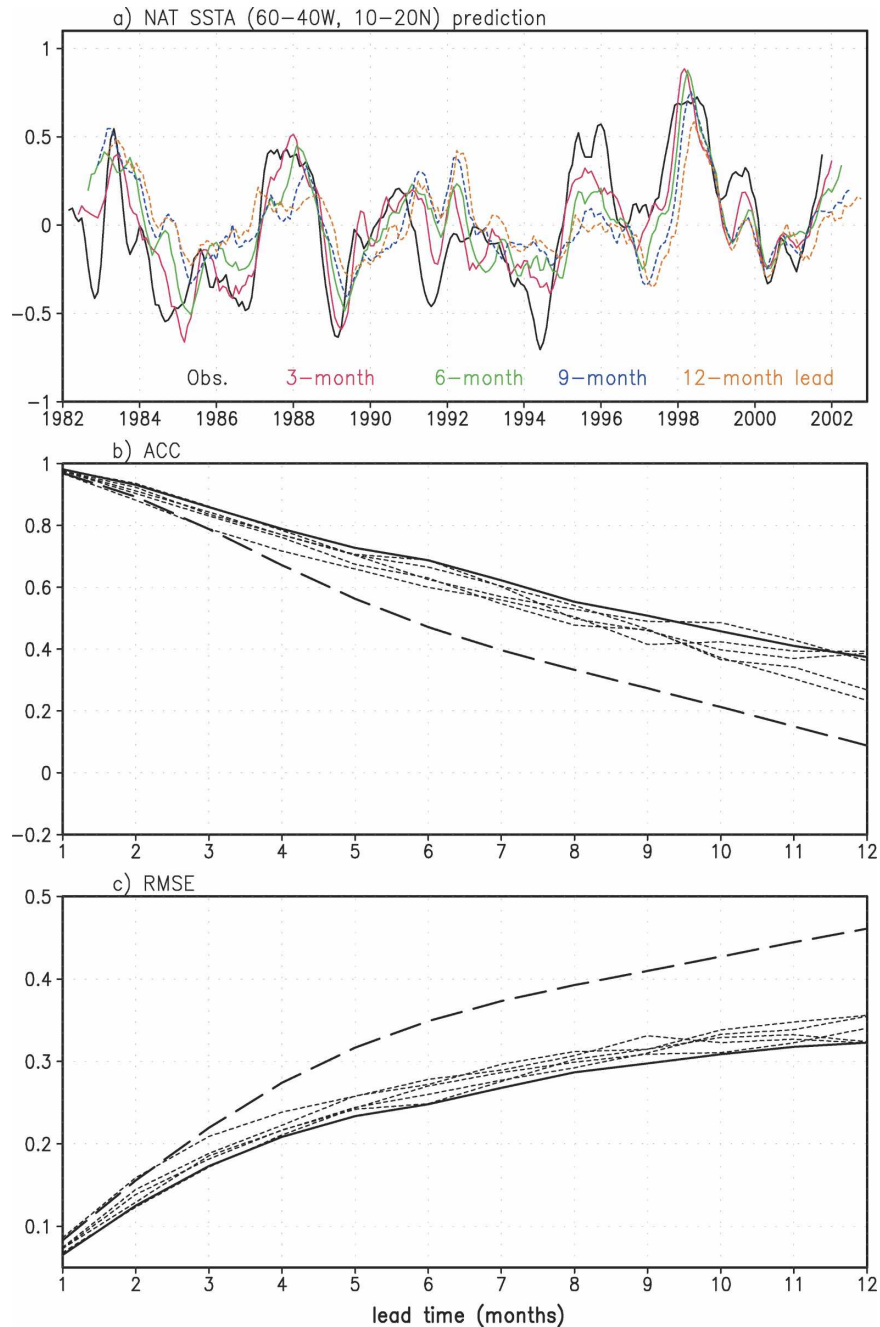


FIG. 14. Same as in Fig. 5, but for the observed and predicted SST anomalies in the tropical North Atlantic ( $10^{\circ}$ – $20^{\circ}$ N,  $60^{\circ}$ – $40^{\circ}$ W).

times. Nevertheless, in some regions, for example, the tropical North Atlantic and southwestern Indian Ocean where the interannual variations are largely affected by ENSO, the model shows significant predictabilities.

Figure 14a shows the SST anomalies in the tropical North Atlantic ( $10^{\circ}$ – $20^{\circ}$ N,  $60^{\circ}$ – $40^{\circ}$ W) from observations and model predictions at 3-, 6-, 9-, and 12-month

lead times. Observations show that the SST anomaly in this region has a maximum positive correlation of 0.48 with the Niño-3.4 SST index at the 6-month lag. The interannual SST changes are largely predicted even at long lead times except for the false alarms of warm events in 1991 and 1992 and a cold event in 1997 (see colored lines in Fig. 14a). The model produces skillful

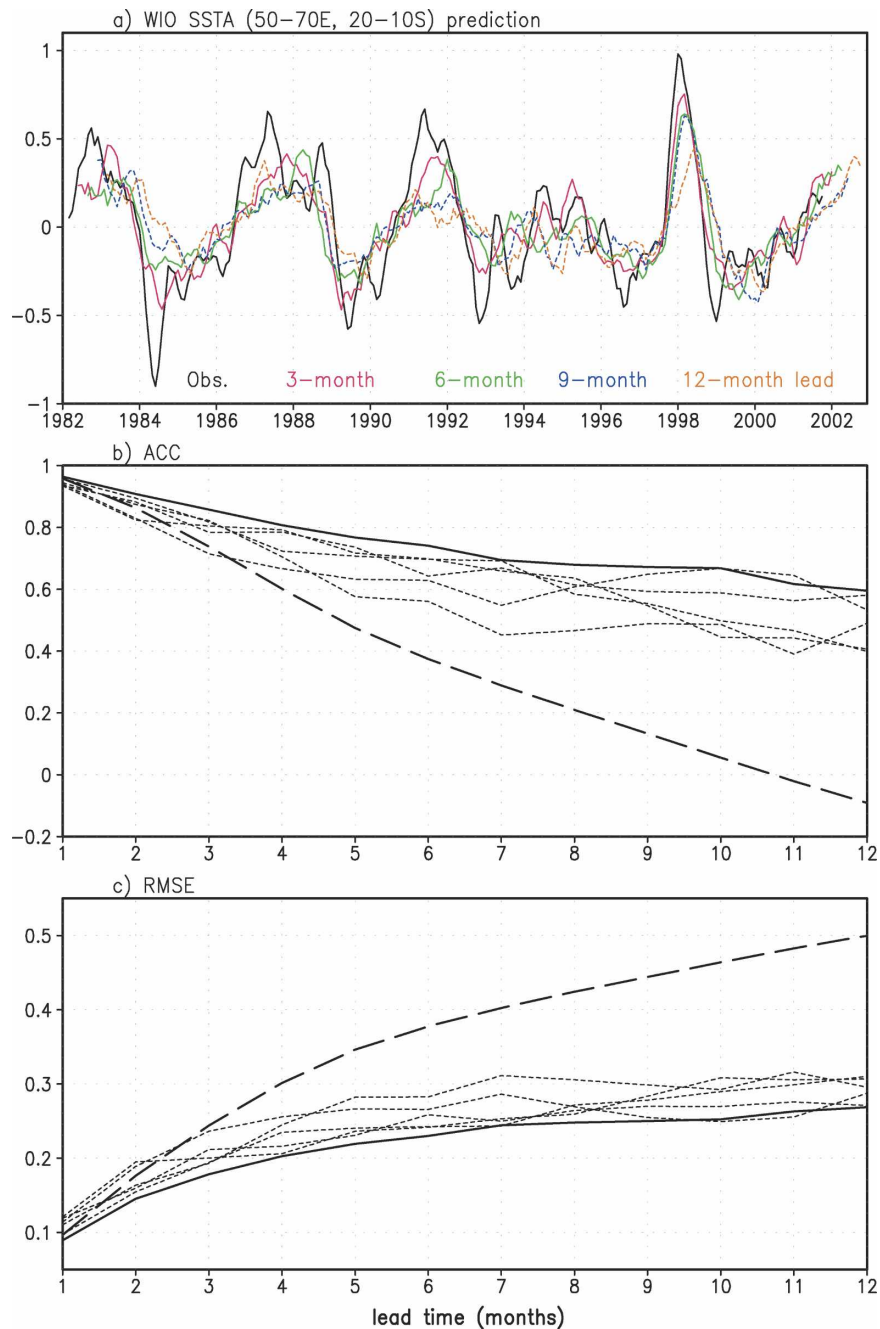


FIG. 15. Same as in Fig. 14, but for the SSTA anomalies in the tropical southwestern Indian Ocean ( $20^{\circ}$ – $10^{\circ}$ S,  $50^{\circ}$ – $70^{\circ}$ E).

predictions until the 7-month lead time with no apparent initial shock (Fig. 14b). The rmses grow as the lead time increases; but they are still smaller than one standard deviation ( $0.34^{\circ}\text{C}$ ) of the observed SSTA until the 12-month lead time (Fig. 14c).

SSTA changes in the tropical southwestern Indian Ocean ( $20^{\circ}$ – $10^{\circ}$ S,  $50^{\circ}$ – $70^{\circ}$ E) show a close relationship

with ENSO (Fig. 15a; see also Xie et al. 2002). The correlation between them reaches 0.63 at the 3-month lag. Correspondingly, the model predicts all interannual variations associated with the past 20-yr ENSO episodes even at the 12-month lead time without any false alarm. The weak signals in 1993–95 in the absence of ENSO events are almost unpredictable. The model

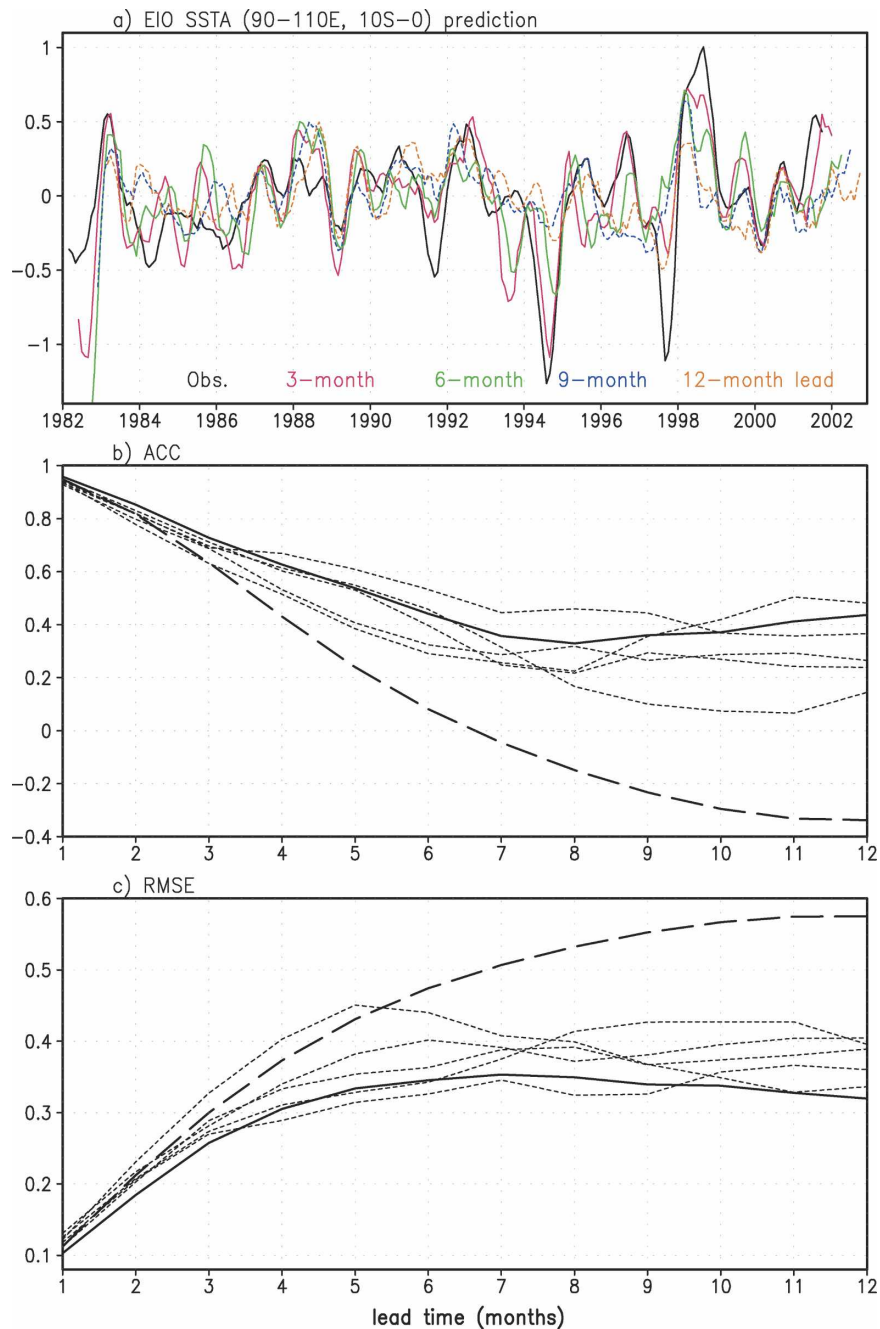


FIG. 16. Same as in Fig. 15, but for the SST anomalies in the eastern equatorial Indian Ocean ( $10^{\circ}\text{S}$ – $0^{\circ}$ ,  $90^{\circ}$ – $110^{\circ}\text{E}$ ).

ACC skill scores of the ensemble mean predictions reach 0.6 at the 12-month lead time (Fig. 15b). Again, there is no apparent initial shock. The rmse's are much smaller than one standard deviation ( $0.34^{\circ}\text{C}$ ) of the observed SST anomaly in this region even for the 12-month lead time predictions (Fig. 15c).

SST in the eastern equatorial Indian Ocean ( $10^{\circ}\text{S}$ – $0^{\circ}$ ,  $90^{\circ}$ – $110^{\circ}\text{E}$ ) shows high-frequency variations (Fig. 16a).

It has very weak negative correlations with the Niño-3.4 SST index at 0- and 1-month lags. This suggests some independence to ENSO (e.g., Saji et al. 1999). The correlations, however, become positive and reach 0.37 at the 7-month lag. The model predicts the high-frequency fluctuations in this region but with a considerable number of false alarms (see colored lines in Fig. 16a). The extreme Indian Ocean dipole (IOD) event in 1994 is

predicted at the 6-month lead time (see also Wajsovicz 2005). The model, however, fails to predict the cold event in 1997. Strong or weak signals associated with the ENSO events, for example, in 1983, 1987, 1989, 1992, 1998, and 2000, are predicted as long as at the 12-month lead time. The model ACC skills decrease rapidly from 0.95 at the 1-month lead time to  $\sim 0.6$  at the 4-month lead time (Fig. 16b). At long lead times, the prediction skills slightly rebound probably due to the delayed ENSO influences. Rmses of the model predictions increase rapidly to about  $0.35^{\circ}\text{C}$  at the 7-month lead time, comparable to one standard deviation of the SST anomaly there (Fig. 16c).

It is interesting that the model also shows a significant predictability near the western coast of Australia (see Fig. 4). SST in that region ( $22^{\circ}$ – $12^{\circ}\text{S}$ ,  $95^{\circ}$ – $115^{\circ}\text{E}$ ) has a weak negative correlation of  $-0.24$  with the Niño-3.4 SST index (see also Fig. 8) with no delayed ENSO influence. Interestingly, SST variations in this region show pronounced decadal signals with a high persistence of  $\sim 0.35$  at the 12-month lag (Figs. 17a,b). Such dominant decadal signals can be predicted at long lead times (see colored lines in Fig. 17a). Model ACC skills reach above 0.6 at the 12-month lead time with rmses smaller than one standard deviation ( $0.38^{\circ}\text{C}$ ; Figs. 17b,c).

We note that the ensemble spread among the five members in the tropical Indian Ocean are larger than those in the Niño-3.4 region and the tropical North Atlantic (see short dashed lines in Figs. 5b, 14b, 15b, 16b, and 17b). This could be related to the strong intraseasonal signals over the equatorial warm SST and the seasonal migration of monsoon winds in the Indian Ocean. Wind stress modifications by the ocean surface current with different coupling physics could be much different in the presence of strong surface wind and ocean current changes.

## 5. Summary and discussion

In this study, we have investigated the seasonal climate/ENSO predictability for the period 1982–2001 based on the SINTEX-F coupled GCM. To produce ensemble forecasts, we have perturbed the coupling physics for each member by taking ocean surface current into account for wind stress calculations in different ways (Luo et al. 2005). This accounts for the uncertainties not only in the initial conditions but also in the model physics. Compatible initial conditions between the atmosphere and ocean are generated using the simple coupled SST-nudging scheme with a strong restoring coefficient to the observations. The initial shock of forecasts has been largely reduced.

The model hindcast results show a high predictability of ENSO. All the warm and cold events in the past 20 yr, including the strongest 1997/98 El Niño episode, are predicted successfully. The model ACC skill scores reach above 0.7 at the 12-month lead time with the rmses much smaller than one standard deviation of the Niño-3.4 SST index. The predicted magnitudes for some particular ENSO events, however, are weakened with a phase delay at mid and long lead times. This seems to be related to the unpredicted intraseasonal wind bursts in the western equatorial Pacific beyond a few months lead. The model also shows a “spring prediction barrier” similar to that in observations as expected from its good capture of seasonal phase locking of ENSO. The spatial pattern of ENSO SST anomalies and teleconnections during the developing (summer), peak (winter), and ending (following summer) phases are predicted at both short and long lead times. Correspondingly, the global drought/flood associated with three ENSO phases are predicted successfully over the 9-month lead time. This implies potential societal impacts of the long lead ENSO forecasts. The negative relationship between the Indian summer monsoon rainfall and ENSO, however, is overestimated in the model predictions. Besides, the model rainfall predictions show systematic biases near the Maritime Continent in the western Pacific. Model calibrations may reduce those systematic biases.

The model results show significant predictabilities in the tropical North Atlantic and southwestern Indian Ocean, where the SST changes are largely affected by ENSO. The ACC scores in the two regions reach about 0.6 at 7- and 12-month lead times, respectively. In the eastern equatorial Indian Ocean, where the local air–sea interactions are active and the signals fluctuate more frequently, the model shows skillful predictions only up to about one season lead. However, the extreme IOD event in 1994 is predicted at the 6-month lead time. Signals associated with the ENSO events are still able to be predicted at long lead times. Interestingly, SST changes near the western coast of Australia can be skillfully predicted at long lead times even without significant ENSO influences. This is due to the dominant decadal signals there.

Success of the coupled nudging scheme for initialization depends crucially on the model performance. Since the SINTEX-F CGCM realistically simulates the climatology and ENSO in the tropical Pacific, the simple SST-nudging scheme is able to generate realistic subsurface information and surface wind changes along the equatorial Pacific including several intraseasonal wind bursts in the west. In the eastern part, however, the model-produced mean thermocline is too shallow. This

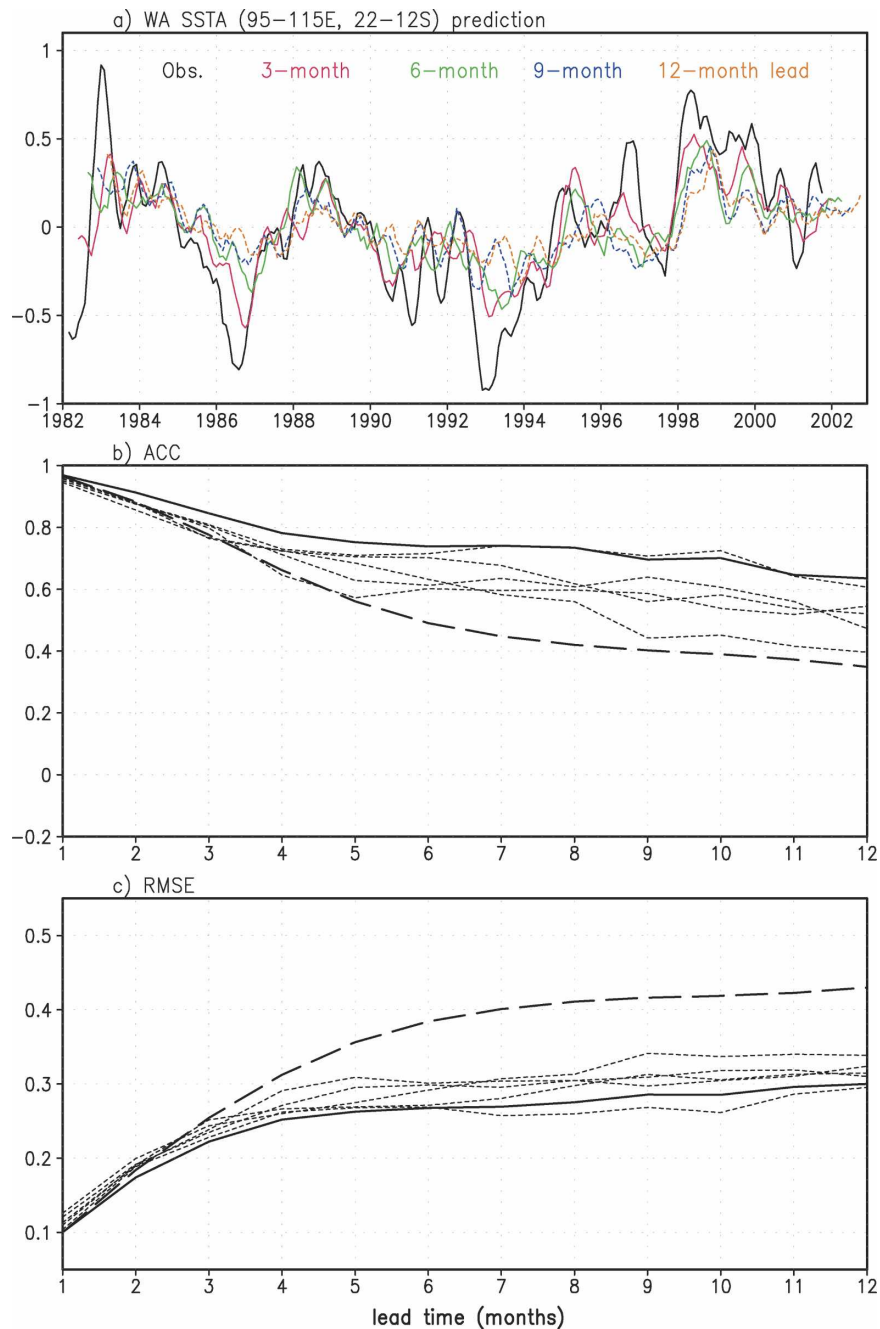


FIG. 17. Same as in Fig. 16, but for the SST anomalies near the western coast of Australia ( $22^{\circ}$ – $12^{\circ}$ S,  $95^{\circ}$ – $115^{\circ}$ E).

affects the climate drifts during forecasts. Away from the equatorial region, where mechanisms for generating subsurface variations are rather complicated, errors in the initial oceanic conditions could be more severe. This tends to affect the ENSO predictions at long lead times. Assimilating subsurface observations into the OGCM in a coupled mode shall reduce those errors substantially. This is to be explored in our future work.

*Acknowledgments.* We thank Gurvan Madec, Erich Roeckner, Fei-Fei Jin, Julia Slingo, and Zhengyu Liu for helpful discussions, and two anonymous reviewers for their valuable comments that helped improve the manuscript. Many European collaborators (e.g., INGV, the MPI-ECHAM group, the LODYC-OPA group, and the CERFACS-OASIS group) have been involved in the development of the SINTEX-F CGCM. NOAA

Optimum Interpolation (OI) SST V2 data were provided by the NOAA–CIRES Climate Diagnostics Center. All experiments have been performed using the Earth Simulator.

## REFERENCES

- Achutarao, K., and K. R. Sperber, 2002: Simulation of the El Niño Southern Oscillation: Results from the Coupled Model Intercomparison Project. *Climate Dyn.*, **19**, 191–209.
- Balmaseda, M. A., D. L. T. Anderson, and M. K. Davey, 1994: ENSO prediction using a dynamical ocean model coupled to statistical atmospheres. *Tellus*, **46A**, 497–511.
- Barnett, T. P., M. Latif, N. Graham, M. Flügel, S. Pazan, and W. White, 1993: ENSO and ENSO-related predictability. Part I: Prediction of equatorial Pacific sea surface temperature with a hybrid coupled ocean–atmosphere model. *J. Climate*, **6**, 1545–1566.
- Barnston, A. G., M. H. Glantz, and Y. He, 1999: Predictive skill of statistical and dynamical climate models in SST forecasts during the 1997/98 El Niño episode and the 1998 La Niña onset. *Bull. Amer. Meteor. Soc.*, **80**, 217–243.
- Blanke, B., and P. Delecluse, 1993: Variability of the tropical Atlantic Ocean simulated by a general circulation model with two different mixed layer physics. *J. Phys. Oceanogr.*, **23**, 1363–1388.
- Cane, M. A., S. E. Zebiak, and S. C. Dolan, 1986: Experimental forecasts of El Niño. *Nature*, **321**, 827–832.
- Carton, J. A., G. Chepurin, and X. Cao, 2000: A Simple Ocean Data Assimilation analysis of the global upper ocean 1950–95. Part II: Results. *J. Phys. Oceanogr.*, **30**, 311–326.
- Charnock, M., 1955: Wind stress on a water surface. *Quart. J. Roy. Meteor. Soc.*, **81**, 639–640.
- Chen, D., S. E. Zebiak, and M. A. Cane, 1997: Initialization and predictability of a coupled ENSO forecast model. *Mon. Wea. Rev.*, **125**, 773–788.
- , M. A. Cane, S. E. Zebiak, R. Cañizares, and A. Kaplan, 2000: Bias correction of an ocean–atmosphere coupled model. *Geophys. Res. Lett.*, **27**, 2585–2588.
- , —, A. Kaplan, S. E. Zebiak, and D. Huang, 2004: Predictability of El Niño over the past 148 years. *Nature*, **428**, 733–736.
- Clarke, A. J., and S. van Gorder, 2003: Improving El Niño prediction using a space–time integration of Indo-Pacific winds and equatorial Pacific upper ocean heat content. *Geophys. Res. Lett.*, **30**, 1399, doi:10.1029/2002GL016673.
- Davey, M., and Coauthors, 2002: STOIC: A study of coupled model climatology and variability in tropical ocean regions. *Climate Dyn.*, **18**, 403–420.
- Dijkstra, H. A., and J. D. Neelin, 1995: Coupled ocean–atmosphere interaction and the tropical climatology. Part II: Why the cold tongue is in the east. *J. Climate*, **8**, 1343–1359.
- Doblas-Reyes, F. J., R. Hagedorn, and T. N. Palmer, 2005: The rationale behind the success of multi-model ensembles in seasonal forecasting. Part II: Calibration and combination. *Tellus*, **57A**, 234–252.
- Fedorov, A. V., S. L. Harper, S. G. Philander, B. Winter, and A. Wittenberg, 2003: How predictable is El Niño? *Bull. Amer. Meteor. Soc.*, **84**, 911–919.
- Gent, P. R., and J. C. McWilliams, 1990: Isopycnal mixing in ocean circulation models. *J. Phys. Oceanogr.*, **20**, 150–155.
- Gualdi, S., A. Navarra, E. Guilyardi, and P. Delecluse, 2003: Assessment of the tropical Indo-Pacific climate in the SINTEX CGCM. *Ann. Geophys.*, **46**, 1–26.
- , A. Alessandri, and A. Navarra, 2005: Impact of atmospheric horizontal resolution on ENSO forecasts. *Tellus*, **57A**, 357–374.
- Guilyardi, E., P. Delecluse, S. Gualdi, and A. Navarra, 2003: Mechanisms for ENSO phase change in a coupled GCM. *J. Climate*, **16**, 1141–1158.
- , and Coauthors, 2004: Representing El Niño in coupled ocean–atmosphere GCMS: The dominant role of the atmospheric component. *J. Climate*, **17**, 4623–4629.
- Hagedorn, R., F. J. Doblas-Reyes, and T. N. Palmer, 2005: The rationale behind the success of multi-model ensembles in seasonal forecasting. Part I: Basic concept. *Tellus*, **57A**, 219–233.
- Ji, M., and A. Leetmaa, 1997: Impact of data assimilation on ocean initialization and El Niño prediction. *Mon. Wea. Rev.*, **125**, 742–753.
- , A. Kumar, and A. Leetmaa, 1994: A multiseason climate forecast system at the National Meteorological Center. *Bull. Amer. Meteor. Soc.*, **75**, 569–577.
- Keenlyside, N., M. Latif, M. Botzet, J. Jungclauss, and U. Schulzweida, 2005: A coupled method for initializing El Niño–Southern Oscillation forecasts using sea surface temperature. *Tellus*, **57A**, 340–356.
- Kirtman, B. P., J. Shukla, B. Huang, Z. Zhu, and E. K. Schneider, 1997: Multiseasonal predictions with a coupled tropical ocean–global atmosphere system. *Mon. Wea. Rev.*, **125**, 789–808.
- Krishnamurti, T. N., C. M. Kishtawal, T. E. LaRow, D. R. Bachiochi, Z. Zhang, C. E. Williford, S. Gadgil, and S. Surendran, 1999: Improved weather and seasonal climate forecasts from multimodel superensemble. *Science*, **285**, 1548–1550.
- Kumar, K. K., B. Rajagopalan, and M. A. Cane, 1999: On the weakening relationship between the Indian monsoon and ENSO. *Science*, **284**, 2156–2159.
- Landsea, C. W., and J. A. Knaff, 2000: How much skill was there in forecasting the very strong 1997/98 El Niño? *Bull. Amer. Meteor. Soc.*, **81**, 2107–2119.
- Latif, M., T. P. Barnett, M. A. Cane, M. Flügel, N. E. Graham, H. von Storch, J.-S. Xu, and S. E. Zebiak, 1994: A review of ENSO prediction studies. *Climate Dyn.*, **9**, 167–179.
- Lengaigne, M., E. Guilyardi, J.-P. Boulanger, C. Menkes, P. Inness, P. Delecluse, and J. M. Slingo, 2004: Triggering of El Niño by westerly wind events in a coupled general circulation model. *Climate Dyn.*, **23**, 601–620.
- Louis, J. F., 1979: A parametric model of vertical eddy fluxes in the atmosphere. *Bound.-Layer Meteor.*, **17**, 187–202.
- Luo, J.-J., S. Masson, S. Behera, P. Delecluse, S. Gualdi, A. Navarra, and T. Yamagata, 2003: South Pacific origin of the decadal ENSO-like variation as simulated by a coupled GCM. *Geophys. Res. Lett.*, **30**, 2250, doi:10.1029/2003GL018649.
- , —, E. Roeckner, G. Madec, and T. Yamagata, 2005: Reducing climatology bias in an ocean–atmosphere CGCM with improved coupling physics. *J. Climate*, **18**, 2344–2360.
- Madec, G., P. Delecluse, M. Imbard, and C. Levy, 1998: OPA 8.1 ocean general circulation model reference manual. LODYC/IPSL Tech. Rep. Note 11, Paris, France, 91 pp.
- McPhaden, M. J., 1999: Genesis and evolution of the 1997–98 El Niño. *Science*, **283**, 950–954.
- Morcrette, J.-J., L. Smith, and Y. Fouquart, 1986: Pressure and temperature dependence of the absorption in longwave radiation parameterizations. *Beitr. Phys. Atmos.*, **59**, 455–469.

- Neelin, J. D., D. S. Battisti, A. C. Hirst, F.-F. Jin, Y. Wakata, T. Yamagata, and S. E. Zebiak, 1998: ENSO theory. *J. Geophys. Res.*, **103**, 14 261–14 290.
- Oberhuber, J. M., E. Roeckner, M. Christopher, M. Esch, and M. Latif, 1998: Predicting the 97 El Niño event with a global climate model. *Geophys. Res. Lett.*, **25**, 2273–2276.
- Pacanowski, R., 1987: Effect of equatorial currents on surface stress. *J. Phys. Oceanogr.*, **17**, 833–838.
- Palmer, T. N., 2001: A nonlinear dynamical perspective on model error: A proposal for non-local stochastic-dynamic parameterization in weather and climate prediction models. *Quart. J. Roy. Meteor. Soc.*, **127**, 279–304.
- , and Coauthors, 2004: Development of a European multi-model ensemble system for seasonal-to-interannual prediction (DEMETER). *Bull. Amer. Meteor. Soc.*, **85**, 853–872.
- Rasmusson, E. M., and T. H. Carpenter, 1982: Variations in tropical sea surface temperature and surface wind fields associated with the Southern Oscillation/El Niño. *Mon. Wea. Rev.*, **110**, 354–384.
- Rayner, N. A., D. E. Parker, E. B. Horton, C. K. Folland, L. V. Alexander, D. P. Rowell, E. C. Kent, and A. Kaplan, 2003: Global analyses of sea surface temperature, sea ice, and night marine air temperature since the late nineteenth century. *J. Geophys. Res.*, **108**, 4407, doi:10.1029/2002JD002670.
- Reynolds, R. W., N. A. Rayner, T. M. Smith, D. C. Stokes, and W. Wang, 2002: An improved in situ and satellite SST analysis for climate. *J. Climate*, **15**, 1609–1625.
- Roeckner, E., and Coauthors, 1996: The atmospheric general circulation model ECHAM-4: Model description and simulation of present-day climate. Max-Planck-Institut für Meteorologie Rep. 218, Hamburg, Germany, 90 pp.
- Rosati, A., K. Miyakoda, and R. Gudgel, 1997: The impact of ocean initial conditions on ENSO forecasting with a coupled model. *Mon. Wea. Rev.*, **125**, 754–772.
- Roulet, G., and G. Madec, 2000: Salt conservation, free surface and varying volume: A new formulation for ocean GCMs. *J. Geophys. Res.*, **105**, 23 927–23 942.
- Saji, N. H., B. N. Goswami, P. N. Vinayachandran, and T. Yamagata, 1999: A dipole mode in the tropical Indian Ocean. *Nature*, **401**, 360–363.
- Schneider, E. K., B. Huang, Z. Zhu, D. G. DeWitt, J. L. Kinter III, B. P. Kirtman, and J. Shukla, 1999: Ocean data assimilation, initialization, and predictions of ENSO with a coupled GCM. *Mon. Wea. Rev.*, **127**, 1187–1207.
- Smith, T. M., A. G. Barnston, M. Ji, and M. Chelliah, 1995: The impact of Pacific Ocean subsurface data on operational prediction of tropical Pacific SST at the NCEP. *Wea. Forecasting*, **10**, 708–714.
- Stockdale, T. N., 1997: Coupled ocean–atmosphere forecasts in the presence of climate drift. *Mon. Wea. Rev.*, **125**, 809–818.
- , D. L. T. Anderson, J. O. S. Alves, and M. A. Balmaseda, 1998: Global seasonal rainfall forecasts using a coupled ocean–atmosphere model. *Nature*, **392**, 370–373.
- Tang, Y., R. Kleeman, A. M. Moore, A. Weaver, and J. Vialard, 2003: The use of ocean reanalysis products to initialize ENSO prediction. *Geophys. Res. Lett.*, **30**, 1694, doi:10.1029/2003GL017664.
- Tiedtke, M., 1989: A comprehensive mass flux scheme for cumulus parameterization in large-scale models. *Mon. Wea. Rev.*, **117**, 1779–1800.
- Tozuka, T., J.-J. Luo, S. Masson, S. K. Behera, and T. Yamagata, 2005: Annual ENSO simulated in a coupled ocean–atmosphere model. *Dyn. Atmos. Oceans*, **39**, 41–60.
- Valcke, S., L. Terray, and A. Piacentini, 2000: The OASIS coupler user guide version 2.4. CERFACE Tech. Rep. TR/CGMC/00-10, 85 pp.
- Wajsowicz, R. C., 2005: Forecasting extreme events in the tropical Indian Ocean sector climate. *Dyn. Atmos. Oceans*, **39**, 137–151.
- Webster, P. J., and S. Yang, 1992: Monsoon and ENSO: Selectively interactive systems. *Quart. J. Roy. Meteor. Soc.*, **118**, 877–926.
- Xie, P., and P. A. Arkin, 1996: Analyses of global monthly precipitation using gauge observations, satellite estimates, and numerical model predictions. *J. Climate*, **9**, 840–858.
- Xie, S.-P., H. Annamalai, F. A. Schott, and J. P. McCreary, 2002: Structure and mechanisms of South Indian Ocean climate variability. *J. Climate*, **15**, 864–878.
- Xu, Y., M. A. Cane, S. E. Zebiak, and M. B. Blumenthal, 1994: On the prediction of ENSO: A study with a low-order Markov model. *Tellus*, **46A**, 512–528.